Journal of Translational Medicine

RESEARCH

Open Access

RNA cargo profiling of muscle extracellular vesicles identifies candidate biomarkers of disease activity and muscle degeneration in FSHD

Elvira Ragozzino[1*†], Sara Bortolani[2†], Lorena Di Pietro[1,3], Elisa Orecchini[1,4], Andrea Papait[1,3], Simona Nanni[3,5], Eleonora Torchia[2], Mauro Monforte[2], Beatrice Ravera[2], Luciano Giacò[4], Giulia Mantini[4], Annalaura Torella[6,7], Vincenzo Nigro[6,7], Diego Sibilia[1,3], Gurjit Kaur[1], Flavia Giacalone[1], Andrea Sabino[8], Manuela Papacci[8], Alberto Augello[3], Donatella Lucchetti[5,9], Alessandro Sgambato[5,9], Giorgio Tasca[10], Valentina Saccone[1,3], Wanda Lattanzi[1,3], Ornella Parolini[1,11†] and Enzo Ricci[2,8†]

Abstract

Background Facioscapulohumeral muscular dystrophy (FSHD) is a progressive neuromuscular disorder characterized by high inter- and intra-individual variability in muscle involvement, disease severity, and rate of progression, even among affected relatives. Remarkably, asymptomatic relatives of FSHD patients, referred to as non-penetrant gene carriers, remain clinically unaffected throughout their lives, despite carrying the genetic background sufficient to cause FSHD. The clinical heterogeneity of FSHD, together with the increasing number of clinical trials involving FSHD patients, underscores the urgent need for reliable biomarkers enabling disease monitoring, stratification of patients and evaluation of treatment efficacy. Extracellular vesicles (EVs) have emerged as promising biomarkers since their cargo reflects physiological state of muscle tissue and remains stable into bloodstream.

Methods To explore their potential in FSHD, we isolated EVs from ex-vivo muscle explants obtained from a cross-sectional cohort of 22 FSHD patients, 4 non-penetrant gene carriers and 6 healthy controls. EV-RNA cargo was profiled using small RNA and total RNA sequencing.

Results Our exploratory study identified distinct EV-RNA signatures, including microRNA, isomiRs and long transcripts, associated with disease activity, assessed by short-tau inversion recovery signal on magnetic resonance imaging (MRI). Our analyses also identified EV-RNA profiles linked to muscle degeneration, assessed by T1-weighted signal on (MRI). A preliminary investigation of the identified EV-RNA profiles also showed an association with the presence or absence of T1 progression at 2-year MRI follow-up.

†Elvira Ragozzino, Sara Bortolani, Ornella Parolini, & Enzo Ricci contributed equally to this work.

*Correspondence:
Elvira Ragozzino
elvira.ragozzino@unicatt.it

Full list of author information is available at the end of the article

Conclusions In this exploratory study, we present a comprehensive characterization of RNA cargo from muscle EVs in FSHD. The identification of EV-RNA signatures linked to disease activity and muscle degeneration supports their evaluation as potential non-invasive biomarkers for disease monitoring, with validation in systemic circulation and in larger cohorts needed to assess their potential contribution to clinical trial design. Moreover, these findings provide novel insights into FSHD disease mechanisms.

Keywords Facioscapulohumeral muscular dystrophy, Extracellular vesicles, Magnetic resonance imaging, Transcriptomic profiling, RNA cargo, Disease biomarkers

Background

Facioscapulohumeral muscular dystrophy (FSHD) is an autosomal dominant neuromuscular disorder with an estimated prevalence of 1 in 15,000 individuals, ranking as the third most common muscular dystrophy worldwide. [1] A defining feature of FSHD is its variable pattern of muscle involvement, whereby specific muscles remain unaffected despite lifelong disease. [2] FSHD displays also pronounced inter-individual variability in age at onset, disease severity, and progression rate, even among affected relatives. [2] Moreover, asymptomatic relatives of FSHD patients, referred to as non-penetrant gene carriers (NPGC), remain clinically unaffected throughout their lives despite carrying the genetic background sufficient to cause FSHD. [3] FSHD is an epigenetic disorder as the most prevalent form, FSHD1, is caused by the shortening of the D4Z4 macrosatellite region on chromosome 4q35, which leads to the aberrant expression of the *double homeobox 4* (*DUX4*) gene in the presence of a permissive 4qA haplotype. [1, 4] DUX4 is a homeotic transcription factor that plays a crucial role during the early cell divisions of the embryo. However, after this initial phase, it is silenced in all adult tissues except the gonads. [1] Despite the mechanism by which ectopic DUX4 expression drives selective muscle degeneration remains partially understood, therapeutic strategies targeting this pathway are currently been evaluated in clinical trials. [5] Magnetic resonance imaging (MRI) is a useful tool for evaluating muscle involvement and disease progression in FSHD. [6–9] Affected muscles may show various degrees of fatty replacement on T1-weighted (T1) sequences either or not associated with hyperintense lesions on short-tau inversion recovery (STIR) sequences, representing edematous alterations. [10–12] Longitudinal MRI studies have shown that STIR-positive (STIR+) muscles degenerate more rapidly than STIR-negative (STIR-) muscles, indicating an active disease phase serving as a prognostic biomarker for FSHD. [13–16] STIR+ muscles in FSHD patients are characterized by inflammation [17, 18], increased fibrosis [18, 19], dysregulation of the non-myogenic mesenchymal cell population [15], and a higher propensity to express DUX4 and its target genes. [13, 20, 21] Despite numerous protein and RNA biomarker candidates have been proposed for FSHD [20, 22–32], no circulating biomarker has reliably correlated with STIR-positivity. [13–15] This gap highlights the need for biomarkers capable of capturing early, MRI-detectable disease activity and reflecting the molecular processes occurring within affected muscles. Recent advances in the study of extracellular vesicles (EVs) offer a promising avenue to address this issue. [33] EVs are membrane-bound particles secreted by cells via paracrine or exocrine mechanisms, enabling intercellular communication while protecting their cargo from enzymatic degradation. [34] The molecular composition of EV cargo, including proteins, nucleic acids, and lipids, reflects the physiological or pathological status of the tissue of origin. [34] As observed in other organs, skeletal muscle-derived EVs are released into circulation, allowing them to play a role in systemic communication. [35] Consequently, EV cargoes are well-suited to be used for monitoring the dynamics of biological processes, including treatment responses in chronic diseases such as muscular dystrophies. [36–39] However, despite increasing interest in EVs across neuromuscular disorders, no study has yet defined whether EVs released directly from FSHD muscles carry molecular signatures that mirror MRI features. Moreover, it remains unknown whether EV-derived RNA cargo can distinguish active disease from chronic degeneration, or predict future progression, representing a major unmet need in FSHD biomarker research. Here, we hypothesize that EVs released directly from FSHD STIR+ muscles carry distinct molecular signatures that correlate with MRI status. In this study, we characterized the small- and long-RNA profiles of EVs isolated from muscles of FSHD patients with distinct degree of involvement on MRI, NPGC and healthy controls (CTRL). We discovered distinct RNA signatures associated with STIR-positivity, a marker of disease activity, and found that EV-RNA cargo also varies with T1-positivity, reflecting muscle degeneration. Finally, we explored whether baseline expression levels of these candidate EV-RNA biomarkers could be associated to disease progression over a two-year MRI follow-up.

Methods

Patients' enrollment and specimen collection

This study was designed as a cross-sectional analysis of EV cargo in FSHD muscle biopsies collected at baseline. A subset of samples was subsequently stratified based

on the availability of 2-year MRI follow-up data, allowing retrospective assessment of associations between EV biomarkers and longitudinal disease progression. Specifically, twenty-two FSHD patients with a confirmed FSHD1 diagnosis were enrolled in this study, among the patients routinely followed-up at Fondazione Policlinico Universitario Agostino Gemelli IRCCS. Four asymptomatic relatives of FSHD patients with a positive genetic testing for FSHD, referred to as NPGC, and 6 age-matched CTRL, with no past and current history of systemic inflammatory disease, were also enrolled [mean age CTRL ± standard deviation (SD): 53 ± 8 years, mean age NPGC ± SD: 49 ± 7 years, mean age FSHD patients ± SD: 43 ± 15 years] (Table 1). No a priori power calculation was performed due to the exploratory nature of the study and the limited availability of muscle explants. All FSHD patients and NPGC underwent muscle magnetic resonance imaging before performing conchotome muscle biopsy as previously described [40], to guide muscle selection. Biopsied muscles of FSHD patients were chosen based on their MRI characteristics, to sample those with hyperintense (STIR+) or normal (STIR-) signals on STIR sequences, as well as those with hyperintense (T1+) or normal (T1-) signals on T1 sequences. Two neurologists with experience in muscle imaging (E. Ricci; SB) independently assessed all the scans. Muscle biopsy was performed within 2 weeks from the first MRI scan after obtaining signed informed consent. Baseline T1 sequences were first evaluated using a 5-point semiquantitative scale (named T1-score) to assess the extent of fatty replacement in single muscles (0 = normal appearance; 1 = traces of increased signal intensity; 2 = increased signal intensity with beginning confluence in less than 50% of the muscle; 3 increased signal intensity in more than 50% of an examined muscle; 4 = the entire muscle is replaced by increased signal intensity) for FSHD patients (22/22) and NPGC (4/4). [41] Longitudinal T1 sequences evaluation was performed for the available follow-up scans of

Table 1 Informative data of enrolled subjects and skeletal muscles

						RNA sequencing			Baseline			2-year
Group	**Patient (number)**	**Age (years)**	**Sex**	**EcoR1**	**Muscle**	**microRNAs**	**IsomiRs**	**Long RNAs**	**STIR**	**T1**	**CSS**	**T1 progression**
CTRL	CTRL#1	56	M	/	vastus lateralis	no	no	yes	/	/	/	/
	CTRL#2	36	M	/	vastus lateralis	yes	yes	no	/	/	/	/
	CTRL#3	49	M	/	vastus lateralis	yes	yes	yes	/	/	/	/
	CTRL#4	61	F	/	vastus lateralis	yes	yes	yes	/	/	/	/
	CTRL#5	57	M	/	vastus lateralis	yes	yes	no	/	/	/	/
	CTRL#6	57	M	/	vastus lateralis	yes	yes	no	/	/	/	/
NPGC	FSHD#1	49	F	28	vastus lateralis	yes	yes	yes	negative	0	0	no
	FSHD#2	39	F	28	vastus lateralis	yes	yes	yes	negative	0	0	no
	FSHD#3	55	F	33	vastus lateralis	yes	yes	yes	negative	0	0	/
	FSHD#4	51	M	28	vastus lateralis	yes	yes	no	negative	0	0	no
STIR-	FSHD#5	60	M	26	vastus lateralis	no	no	yes	negative	2	4	no
	FSHD#6	62	F	25	vastus lateralis	no	no	yes	negative	0	4	no
	FSHD#7	34	M	23	vastus lateralis	no	no	yes	negative	0	1	no
	FSHD#8	57	M	26	vastus lateralis	yes	yes	yes	negative	0	3	no
	FSHD#9	49	F	19	vastus lateralis	yes	yes	no	negative	0	1,5	no
	FSHD#10	59	F	28	vastus lateralis	no	no	yes	negative	2	3	no
	FSHD#11	42	M	18	vastus lateralis	yes	yes	no	negative	0	2	no
	FSHD#12	57	M	26	vastus lateralis	yes	yes	yes	negative	0	3	/
	FSHD#13	22	M	30	vastus lateralis	yes	yes	no	negative	0	2,5	/
	FSHD#14	37	M	23	vastus lateralis	yes	yes	yes	negative	0	1,5	/
	FSHD#15	23	F	53	vastus lateralis	no	no	yes	negative	1	4	/
	FSHD#16	25	M	25	vastus lateralis	yes	yes	no	negative	0	1	no
STIR+	FSHD#17	60	M	24	vastus lateralis	yes	yes	yes	positive	1	2,5	no
	FSHD#18	33	F	17	vastus lateralis	yes	no	yes	positive	1	4	yes
	FSHD#19	47	M	22	vastus lateralis	no	no	yes	positive	2	3,5	/
	FSHD#20	22	M	26	gastrocnemius	no	no	yes	positive	3	1,5	yes
	FSHD#21	70	M	29	vastus lateralis	no	no	yes	positive	2	1,5	yes
	FSHD#22	34	M	27	gastrocnemius	yes	yes	yes	positive	1	3	yes
	FSHD#23	27	M	27	tibialis anterior	yes	yes	no	positive	0	2,5	yes
	FSHD#24	54	M	24	vastus lateralis	yes	yes	yes	positive	2	4	yes
	FSHD#25	37	M	23	vastus lateralis	yes	yes	no	positive	0	4	yes
	FSHD#26	54	M	30	gastrocnemius	yes	yes	no	positive	0	2,5	no

patients' muscles (8/12 STIR- and 9/10 STIR+ muscles). To detect more subtle changes not identified by the former assessment, the observers performed a direct visual comparison between the baseline and the follow-up scan of each patient on the same computer monitor as previously described. [14] Radiological progression in single muscles was defined as an increase in fatty replacement at 2-year MRI scans. All protocols were conducted according to the European Good Clinical Practice guidelines after the approval by the Ethical Committee of the Fondazione Policlinico Universitario Agostino Gemelli IRCCS, Università Cattolica del Sacro Cuore (protocol ID 4973), and upon obtaining the written informed consent.

Isolation of EVs from skeletal muscle biopsies

Immediately after the biopsy procedure, muscle specimens were minced and cultured for 24 hours in M199 medium (Sigma Aldrich) supplemented with 37.5% of EV-depleted fetal bovine serum (FBS, Gibco) and 1% penicillin/streptomycin (Invitrogen). Specifically, EV-depletion from FBS was performed by 120,000 × g ultracentrifugation for 16 hours at 4 °C. [42] The conditioned medium of muscle explant culture was 0.22 µm filtered and centrifuged at 750 × g for 15 minutes to discard debris. EVs were isolated by Total Exosome Isolation Kit from Cell Culture Media (Invitrogen) following manufacturer's instructions and the EV-enriched pellet was resuspended in 200 µL of phosphate buffered saline (PBS, Euroclone) and stored at −80 °C until RNA extraction. The explant approach may introduce ex-vivo alterations in EV secretion, and this limitation was considered during data interpretation.

Nanoparticle tracking analysis

Particle size and concentration was measured by Nanoparticle Tracking Analysis (NTA) using the Nanosight LM10 instrument (Malvern Instruments Ltd) with a 488 nm laser. EV-fraction were diluted 1:1000 in PBS, to obtain the recommended particle concentration (20–120 particles/frame), before injecting into the sample chamber using an automated syringe pump set to capture 5x measurements at 60s long per run (camera level 16). The software used for data capture and analysis was NTA 3.4 Build 3.4.4. Temperature was kept constant at 22 °C.

Scanning electron microscopy

EV morphology was visualized using scanning electron microscopy (SEM). Muscle-derived EVs were diluted 1:20 and fixed in 2,5% (v/v) glutaraldehyde and paraformaldehyde for 30 min at room temperature (RT), followed by centrifugation at 21,500 × g for 10 min at 4 °C. The EV pellet was washed three times in PBS, each followed by centrifugation at 21,500 × g for 10 min at 4 °C. Subsequently, the pellet was treated with osmium tetroxide (3%) for 30 min at RT and centrifuged again under the same conditions. Dehydration was performed through sequential incubations in graded ethanol solutions (30, 50, 70 and 90%) for 5 min each, followed by centrifugation at 21,500 × g for 10 min at 4 °C. The pellet was then incubated twice in 100% (v/v) ethanol for 10 min at RT, with centrifugation after each step, and finally a 30 µL aliquot was collected and deposited onto 10 mm diameter glass coverslips (0.13–0.16 mm thick, CARLO ERBA). The sample was allowed to dry at RT and then mounted on aluminum supports using double-sided carbon tape. Prior to imaging, the sample was sputter-coated with a 10 nm layer of platinum. SEM images were acquired using a Supra 25 microscope (Zeiss, Germany) in In-Lens secondary electron mode, with 10 keV electrons, scan speed 4, and line averaging ($n = 3$) for noise reduction, with a working distance of 1 mm.

Western blot

EVs were lysed for protein extraction in 0,125% NP-40/PBS buffer by vortexing every 10 minutes for 1 hour while incubating the samples on ice. Protein from whole muscle tissue was extracted using RIPA buffer [50 mM Tris–HCl (pH 7,5), 150 mM NaCl, 1% Triton X-100, 0,5% sodium deoxycholate, 0,1% SDS, protease inhibitor, 1 mM NaF, and 1 mM $NaVO_3$]. Proteins in EV cargo and muscle lysate were quantified using the BCA protein assay (23235 Thermo Fisher Scientific). Equal amounts (20 µg) of total proteins from each EV sample (CTRL, NPGC, FSHD STIR–, FSHD STIR+) and from whole muscle were loaded and separated by SDS–PAGE in a 10% precast gel (Bio-Rad) and blotted to nitrocellulose membrane (Bio-Rad). Membranes were blocked with either 5% (w/v) non-fat dry milk (70166 Sigma-Aldrich) or 5% (w/v) BSA (A7030 Sigma-Aldrich) in TBS-0,1% Tween-20, depending on the primary antibody used, and incubated overnight at 4 °C with the following primary antibodies: rabbit anti-CD63 (1:300, H-193, Santa Cruz Biotechnology), mouse anti-Alix (3A9, 1:500, Cell Signaling Technologies #2171), rabbit anti-CD81 (B-11, 1:200, sc-166029, Santa Cruz Biotechnology), rabbit anti-Flotillin-1 (1:200, H-104, Santa Cruz Biotechnology), and rabbit anti-Calnexin (CANX; 1:1000, NB100-1965, Novus Biologicals). After three TBS-T washes, membranes were incubated for 1 hour RT with HRP-conjugated secondary antibodies [(1:1000) Goat anti-Rabbit A120-101P, Goat Anti-Mouse A90-116P, Fortis Life Sciences] diluted in the appropriate blocking solution (milk or BSA). After three washes, membranes were incubated with ECL solution (32106, ThermoFisher) and protein bands were visualized using the ChemiDoc Image system (Bio-Rad).

EV-RNA extraction and RNA sequencing

Total RNA was isolated from 150 µl of EVs using Trizol reagent (Thermo Fisher Scientific), following manufacturer's procedures. RNA quantity was assessed using the QFX fluorimeter (De Novix) and sample integrity was analyzed with the Agilent Bioanalyzer 2100 using Eukaryote Total RNA Pico kit (Agilent Technologies). An amount of 35 ng of total EV-RNA was used to prepare libraries using the SMARTer smRNAseq kit (Takara) and the transcriptomic profile was deep-sequenced using the Illumina NextSeq550Dx platform to evaluate small RNAs (< 200 nucleotides). An amount of 70 ng of total EV-RNA was used to prepare libraries using the TruSeq Stranded Total RNA Sample Prep Kit with Ribo-Zero ribosomal RNA reduction chemistry (Illumina, San Diego, CA) and the transcriptomic profile was also sequenced using the Illumina NextSeq550Dx platform to evaluate long transcripts (> 200 nucleotides). Based on sample availability, EV-RNA was used to perform either small and total RNA sequencing (RNA-seq) or only one of the two, as specified in Table 1. The small RNA-seq yielded an average of 20 million reads per sample, with approximately 81% of the reads mapped to the human genome (GRCh38_p13). The length distribution of the sequenced reads was around 35 nucleotides, and the mapped reads were associated with 11 classes of small RNAs. For total RNA-seq, each sample yielded an average of 42 million reads, with a read length distribution centered around 150 nucleotides.

Bioinformatic analysis

Profile of EV-small RNAs (transcripts < 200 nucleotides) were analyzed through sRNAbench tool. [43] Reads were trimmed with cutadapt. [44] The alignment was performed by sRNAbench tool using the GRCh38_p13 reference genome and annotated with microRNA (miRNA) databases (e.g. miRBase 22, TarBase). Raw counts were normalized, and differential analysis was performed with "edgeR" R library including adjustment of p-values for multiple testing using the Benjamini–Hochberg False Discovery Rate (FDR) method. FDR adjusted p-values did not reach statistical significance, and a cut-off of p-value < 0.05 and |logFC| > 0.5 were used. Differentially expressed miRNAs (DEmiR) were mapped to their target genes ("MultimiR" R package) to subsequently study the involved pathways ("ClusterProfiler" and "RRVGO" R package). Gene Ontology (GO) and Kyoto Encyclopedia of Genes and Genomes (KEGG) pathways were investigated using custom in-house R scripts. Batch correction and differentially expressed isomiRs (DEisomiR) were performed as described for miRNA analysis, setting a cut-off of p-value < 0.05 and the |log2FC| > 0.5. For total RNA-seq (transcripts > 200 nucleotides), raw reads from whole transcriptome libraries were trimmed from TAKARA adapters and aligned to the GRCh38 assembly using STAR mapping tool. [45] All processes were performed on high-performance computing (HPC). Quality checks on raw and normalized counts were performed on R Studio (version 4.3.2). Low abundance genes were excluded from further analysis. Batch correction, differentially expressed gene (DEG) and enrichment analyses were performed as described above for miRNA analysis, setting a cut-off of p-value < 0.05 and the |log2FC| > 0.58. Statistical analysis was performed in RStudio (v4.3.2). The Shapiro–Wilk test was performed for normality and Levene's test for homogeneity of variance. ANOVA followed by Tukey's post-hoc test was applied to normally distributed data with equal variances, while Welch's ANOVA and Games–Howell post-hoc test was used for normal data with unequal variances. For non-normally distributed data, the Kruskal–Wallis test was used, followed by Dunn's post-hoc test and p-value was adjusted using the Bonferroni correction. Correlation analysis was performed using Spearman's test.

Results

Isolation and characterization of FSHD patients' muscle-derived EVs

We isolated EVs from skeletal muscle biopsies of 22 FSHD patients, 4 NPGC and 6 CTRL. Muscle biopsies from FSHD patients were classified based on MRI examination as STIR+ or STIR-, depending on the presence or absence of oedema/inflammation, and further categorized as T1+ or T1-, according to the presence or absence of fat infiltration. Table 1 summarizes participant demographics, MRI-based muscle classifications and the analyses performed. Immediately after biopsy, we cultured muscle explants for 24 hours in EV-depleted medium and isolated the EV-enriched fraction (Fig. 1A). NTA (Fig. 1B) showed that muscle-derived EVs had mean diameters of 123 ± 22 nm in CTRL, 127 ± 26 nm in NPGC, 143 ± 35 nm in FSHD STIR − and 131 ± 38 nm in FSHD STIR+ samples, consistent with the expected size range of small EVs (Fig. 1B). SEM analyses of fixed muscle-derived EVs showed round-shaped morphology ranging from 100 to 150 nm in size (Fig. 1C), in agreement to NTA results (Fig. 1B). Western blot analysis confirmed the presence of EV markers (CD63, ALIX, CD81, Flotillin-1) in muscle-derived EVs, with negligible calnexin contamination compared to whole muscle lysate (Fig. S1A).

M: male, F: female, T1: T1-score. Baseline: radiological and clinical assessments at the time of the biopsy procedure. EcoRI indicates the fragment length of the D4Z4 repeat on chromosome 4q35. CSS: clinical severity score, a 10-point scale used to assess the extent of muscle weakness. CSS ≤ 2.5 = upper-limb involvement only; CSS ≥3 = upper and lower limb involvement. Based on data availability, T1-score was assessed at 2-year MRI

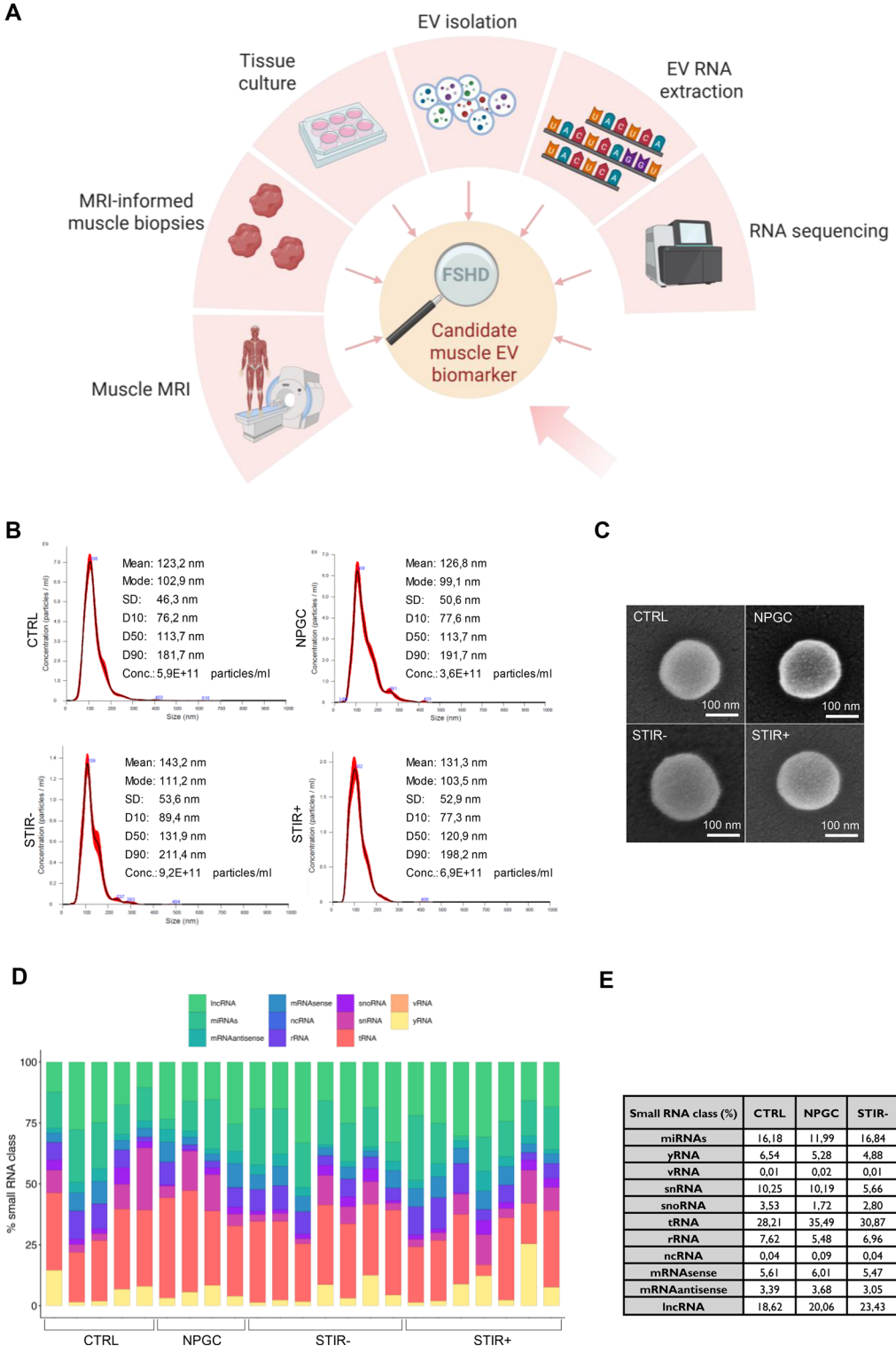

E

Small RNA class (%)	CTRL	NPGC	STIR-	STIR+
miRNAs	16,18	11,99	16,84	15,12
yRNA	6,54	5,28	4,88	8,55
vRNA	0,01	0,02	0,01	0,02
snRNA	10,25	10,19	5,66	7,73
snoRNA	3,53	1,72	2,80	2,89
tRNA	28,21	35,49	30,87	23,16
rRNA	7,62	5,48	6,96	8,13
ncRNA	0,04	0,09	0,04	0,04
mRNAsense	5,61	6,01	5,47	6,47
mRNAantisense	3,39	3,68	3,05	4,06
lncRNA	18,62	20,06	23,43	23,83

Fig. 1 Characterization of EVs from muscle biopsies and their small RNA cargo. (**A**) schematic representation of the experimental plan to isolate extracellular vesicles (EVs) from muscle biopsies and profile their RNA cargo. The figure is created with Biorender.com (**B**) representative size versus concentration distribution graphs of CTRL ($n=5$), NPGC ($n=4$), FSHD STIR- ($n=5$), and FSHD STIR+ ($n=5$) EV samples analysed by Nanosight. (**C**) illustrative scanning electron micrographs of CTRL, NPGC, FSHD STIR- and FSHD STIR+ EV samples. Scale bar = 100 nm. (**D**) the barplots show the percentage of small RNA categories across individual EV samples. Each RNA class is represented by a different color. The Y-axis indicates the relative abundance (%), while the X-axis lists each sample. (**E**) the table shows the average percentage of small RNA classes among CTRL, NPGC, FSHD STIR- and FSHD STIR+ EV samples. Groups were compared using Kruskal-Wallis test

follow-up to define muscles with (yes) or without (no) progression.

Small RNA-seq on muscle EV-cargo

To characterize the RNA cargo of muscle-derived EVs, we extracted total EV-RNA and performed both small (< 200 nt) and long (> 200 nt) RNA-seq. The small RNA-seq analysis was performed on $n = 7$ FSHD STIR+, $n = 7$ FSHD STIR-, $n = 4$ NPGC and $n = 5$ CTRL muscle-derived EVs. The reads mapped to 11 classes of small RNAs, consistent with known EV-RNA cargo profiles in all the samples analyzed (Fig. 1D). [46] Transfer RNAs, long non-coding RNAs, and miRNAs were the most abundant classes (Fig. 1D–E). We observed no significant differences in small RNA class distribution across EVs from CTRL, NPGC, FSHD STIR-, and FSHD STIR+ samples (Fig. 1E).

Muscle EV-miRNAs as candidate biomarkers of disease activity

We performed the DEmiR analysis to identify miRNAs significantly dysregulated in FSHD STIR+ EV samples compared to CTRL (Fig. 2A, Table S1), NPGC (Fig. 2B, Table S1) and FSHD STIR- (Fig. 2C, Table S1) EVs. Our analysis identified 30 differentially expressed miRNAs in FSHD STIR+ EVs. Specifically, 3 miRNAs were upregulated and 4 downregulated in FSHD STIR+ compared to CTRL EVs (Fig. 2A, Table S1). One miRNA was upregulated and 18 downregulated in FSHD STIR+ compared to NPGC EVs (Fig. 2B, Table S1), while 9 miRNAs were upregulated and 4 downregulated in FSHD STIR+ compared to FSHD STIR- EVs (Fig. 2C, Table S1). We conducted a correlation analysis between EV-miRNA expression levels and STIR-positivity within the cohort of FSHD muscle samples. This analysis identified 8 miRNAs with positive and 7 with negative correlation to STIR-positivity (Fig. 2D). Then, we integrated data from two independent statistical approaches: the list of upregulated and downregulated EV-miRNAs in FSHD STIR+ samples derived from the DEmiR analysis (Fig. 2A–C, Table S1), and the results of correlation analysis with STIR-positivity (Fig. 2D). This intersection identified 7 upregulated (hsa-mir-130a-3p, hsa-mir-146b-5p, hsa-mir-146a-5p, hsa-mir-382-5p, hsa-mir-655-3p, hsa-mir-409-3p and hsa-mir-337-3p) and 4 downregulated (hsa-mir-16–2-5p, hsa-mir-27b-3p, hsa-mir-30e-5p and hsa-mir-944-3p) EV-miRNAs associated with STIR-positivity. In Table S2 are reported the exclusive and/or shared EV-miRNAs across DEmiRs and correlation analyses. The combined panel of 7 upregulated EV-miRNAs significantly separated FSHD STIR+ samples from FSHD STIR-, NPGC, and CTRL groups (Fig. 2E). The 4 downregulated EV-miRNAs were able to significantly differentiate FSHD STIR+ samples from both FSHD STIR- and NPGC samples (Fig. 2F). To assess whether our selected miRNAs may participate in FSHD-relevant processes such as inflammatory signaling, embryonic and muscle development, epigenetic regulation, carbohydrate and lipid metabolism, and fibrosis we performed GO Biological Process (BP) and KEGG pathway enrichment analyses. GO BP analysis suggested that the target genes of the 7 upregulated EV-miRNAs could be related to carbohydrate metabolism, B and T cell regulation, negative regulation of complement activation, cellular response to type I interferon and developmental processes (Fig. 2G). The target genes of the 4 downregulated EV-miRNAs appear related to similar immune and developmental pathways, with possible involvement in TGF-β/SMAD and epigenetic regulation of gene expression pathways (Fig. 2G). KEGG analysis suggested that the targets of the upregulated EV-miRNAs could be associated with ECM-receptor interaction, signal transduction (Wnt, TGF-β, PI3K-Akt, AMPK), immune signaling (TCR, BCR, IL-17), chromatin remodeling, and apoptosis (Fig. 2H). The targets of downregulated EV-miRNAs showed enrichment in many of these pathways, including signal transduction and cell death, but lacked enrichment for ECM, TLR, chemokine and IL-17signaling (Fig. 2H).

Muscle EV-isomiRs as candidate biomarkers of disease activity

The small RNA-seq analysis revealed that the miRNA group included both canonical miRNAs and their sequence variants, termed isomiRs. We profiled isomiR content in muscle-derived EVs to identify nucleotide modifications that define specific isomiR variants potentially enriched in distinct sample groups. The boxplots showed that EVs from NPGC muscles were significantly enriched in isomiR non-template uridylation (ntU) nucleotidic modification compared to CTRL samples (Fig. 3A), and in multiple variant (mv) nucleotidic modification compared to both CTRL and FSHD STIR- samples (Fig. 3B). In contrast, non-template cytosine addition (ntC), non-template guanine addition (ntG), leading variant 5' extension (lv5pE), leading variant end processing extension (lvepE), leading variant 3' trimming (lv3pT) and leading variant 5' post-transcriptional (lv5pT) isomiR nucleotidic modifications did not show any significant difference (Fig. S2). Next, we conducted the DEisomiR analysis to identify the isomiRs significantly dysregulated in FSHD STIR+ EV samples compared to FSHD STIR-, NPGC, and CTRL groups. We identified 143 differentially expressed isomiRs in FSHD STIR+ EVs. Specifically, 22 isomiRs were upregulated and 11 were downregulated in FSHD STIR+ compared to CTRL EVs (Fig. 3C, Table S3), 8 were upregulated and 80 were downregulated compared to NPGC EVs (Fig. 3D, Table S3), 31 were upregulated and 22 were downregulated compared

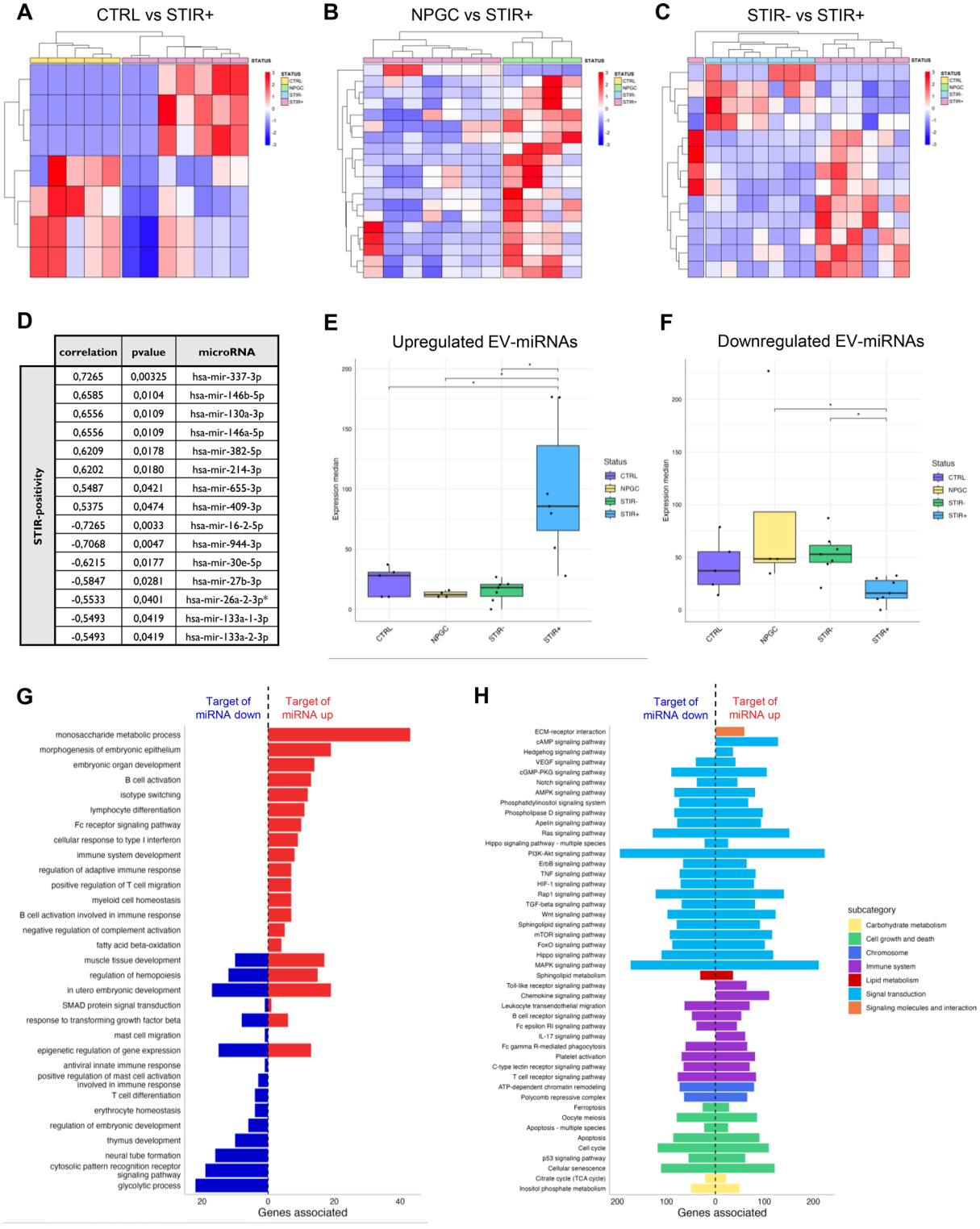

	correlation	pvalue	microRNA
STIR-positivity	0,7265	0,00325	hsa-mir-337-3p
	0,6585	0,0104	hsa-mir-146b-5p
	0,6556	0,0109	hsa-mir-130a-3p
	0,6556	0,0109	hsa-mir-146a-5p
	0,6209	0,0178	hsa-mir-382-5p
	0,6202	0,0180	hsa-mir-214-3p
	0,5487	0,0421	hsa-mir-655-3p
	0,5375	0,0474	hsa-mir-409-3p
	-0,7265	0,0033	hsa-mir-16-2-5p
	-0,7068	0,0047	hsa-mir-944-3p
	-0,6215	0,0177	hsa-mir-30e-5p
	-0,5847	0,0281	hsa-mir-27b-3p
	-0,5533	0,0401	hsa-mir-26a-2-3p*
	-0,5493	0,0419	hsa-mir-133a-1-3p
	-0,5493	0,0419	hsa-mir-133a-2-3p

Fig. 2 Muscle EV-miRNA signature in FSHD STIR+ muscles. Heatmaps of differentially expressed miRNAs between FSHD STIR+ ($n=7$) and CTRL ($n=5$) (**A**), NPGC ($n=4$) (**B**), or FSHD STIR– ($n=7$) EVs (**C**). (**D**) EV-miRNAs significantly correlated with STIR-positivity [Spearman's correlation coefficient (correlation) and p-value reported]. (**E**-**F**) boxplots of 7 upregulated (**E**) and 4 downregulated (**F**) EV-miRNAs resulting from the intersection of DEmiRs and correlation analyses; each dot represents the median expression of selected miRNAs per sample. Groups were compared using the Welch–Games Howell (**E**) and Kruskal–Wallis with Dunn's post hoc test (**F**) (* $p<0.05$; ** $p<0.01$; *** $p<0.001$). (G-H) GO BP (**G**) and KEGG (**H**) enrichment analyses of upregulated (red) and downregulated (blue) EV-miRNA biomarkers. Bar lengths indicate the relative number of predicted target genes associated with each biological process or pathway

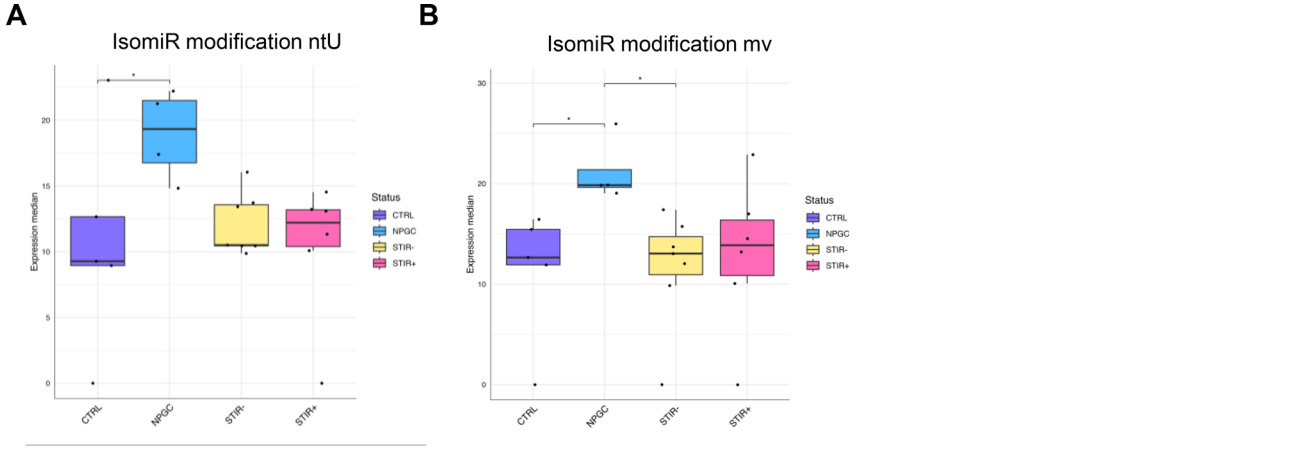

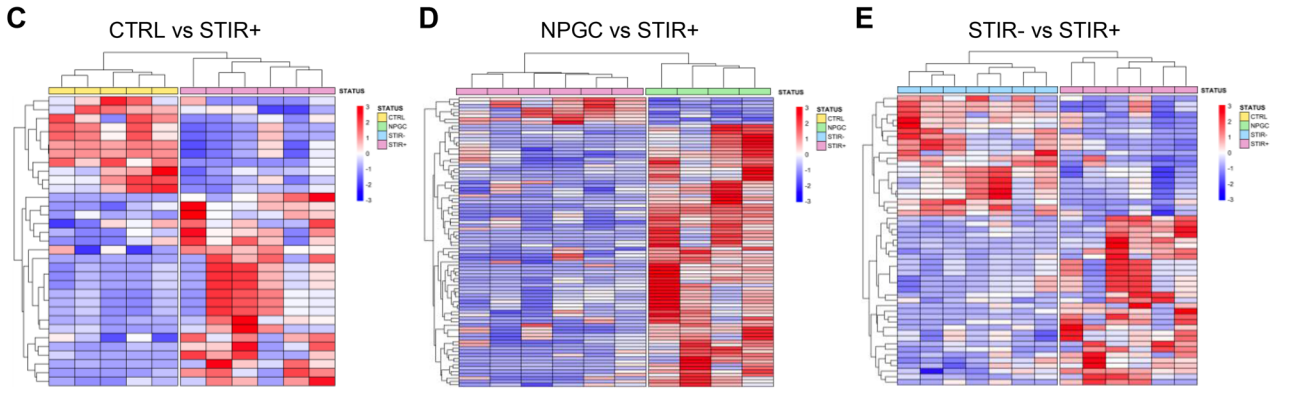

F

	correlation	pvalue	isomiR
STIR-positivity	0,8708	0,00011	hsa-mir-146b-5p#ntC
	0,8660	0,0001	hsa-mir-139-5p#lv3pT
	0,8248	0,0005	hsa-mir-146b-5p#lv3pT
	0,7835	0,0015	hsa-mir-223-3p#mv
	0,7423	0,0037	hsa-mir-103a-2-3p#lv3pT
	0,7423	0,0037	hsa-mir-103a-1-3p#lv3pT
	0,7423	0,0037	hsa-mir-146a-5p#ntC
	0,7423	0,0037	hsa-mir-574-3p#mv
	0,7157	0,0059	hsa-mir-483-3p*#ntC
	0,7052	0,0071	hsa-mir-493-5p#lv3pT
	-0,7423	0,0037	hsa-mir-16-1-5p#lv3pT
	-0,7212	0,0054	hsa-mir-7-1-3p*#ntU
	-0,7109	0,0064	hsa-mir-196b-5p#ntU
	-0,7109	0,0064	hsa-mir-28-5p#ntC
	-0,7011	0,0076	hsa-mir-16-1-5p#lv3pE
	-0,7011	0,0076	hsa-mir-16-1-5p#ntU
	-0,7011	0,0076	hsa-mir-16-2-5p#lv3pT
	-0,7011	0,0076	hsa-mir-16-2-5p#ntU
	-0,6787	0,0107	hsa-mir-30b-5p#ntU
	-0,6691	0,0124	hsa-mir-30c-1-5p#mv

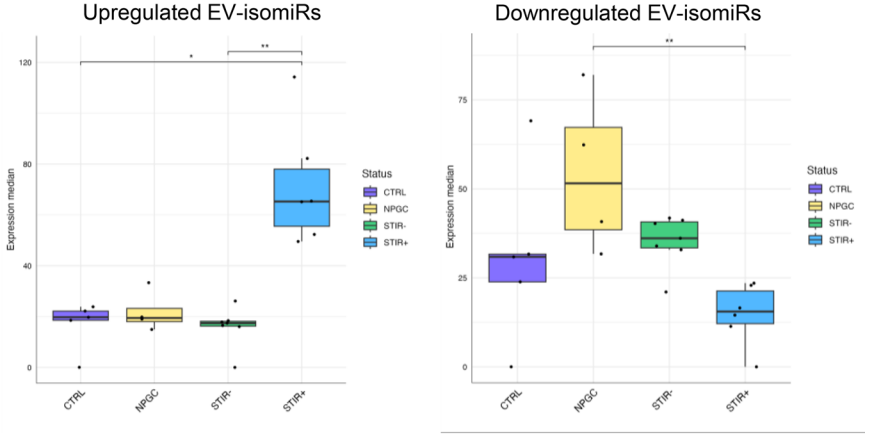

Fig. 3 Muscle EV-isomiR signature in FSHD STIR+ muscles. Boxplots of ntU (**A**) and mv (**B**) nucleotide modifications in muscle EV-isomiRs from CTRL, NPGC, FSHD STIR–, and STIR+ samples. (C-E) heatmaps of differentially expressed isomiRs between FSHD STIR+ ($n=7$) and CTRL ($n=5$) (**C**), NPGC ($n=4$) (**D**), or FSHD STIR– ($n=7$) (**E**). (**F**) top 10 EV-isomiRs significantly correlated with STIR-positivity [Spearman's correlation coefficient (correlation) and p-value reported]. (G-H) boxplots of 19 upregulated (**G**) and 23 downregulated (**H**) EV-isomiRs; each dot represents the median expression of selected isomiRs per sample. Groups were compared using Kruskal–Wallis with Dunn's post hoc test (**G**), one-way ANOVA with Tukey's post hoc test (**H**) (* $p<0.05$; ** $p<0.01$)

to STIR- EVs (Fig. 3E, Table S3). The correlation analysis between EV-isomiRs levels and STIR-positivity across FSHD STIR- and STIR+ samples identified 29 isomiRs with significant positive and 30 with significant negative correlation to STIR-positivity (Table S4). The top 10 positively and negatively correlated EV-isomiRs, ranked by p-value, are shown in Fig. 3F. As for EV-miRNAs, we integrated DEisomiRs and correlation analyses, identifying 19 upregulated and 23 downregulated isomiRs associated with STIR-positivity (Table S5). In Table S6 are reported the exclusive and/or shared EV-isomiRs across DEGs and correlation analyses. The combined panel of 19 upregulated EV-isomiRs effectively separated FSHD STIR+ samples from FSHD STIR-, NPGC, and CTRL groups, showing significant different expression in comparisons between FSHD STIR+ and FSHD STIR-, as well as FSHD STIR+ and CTRL samples (Fig. 3G). Similarly, the 23 downregulated EV-isomiR were also able to differentiate FSHD STIR+ samples from the other groups, with significant different expression observed between FSHD STIR+ and NPGC samples (Fig. 3H).

Muscle EV-long transcripts as candidate biomarkers of disease activity

To characterize the cargo of long RNAs (e.g., transcripts longer than 200 nucleotides) from muscle-derived EVs, we performed total RNA-seq on $n = 7$ FSHD STIR+, $n = 8$ FSHD STIR-, $n = 3$ NPGC and $n = 3$ CTRL samples (Table 1). The DEG analysis identified a total of 561 long transcripts whose expression was significantly dysregulated in STIR+ EVs: 126 long transcripts were upregulated and 156 were downregulated in FSHD STIR+ compared to CTRL EVs (Fig. 4A, Table S7), 179 long transcripts were upregulated and 58 long transcripts were downregulated in STIR+ compared to NPGC EVs (Fig. 4B, Table S7), and 132 long transcripts were upregulated and 25 downregulated in STIR+ compared to STIR- EVs (Fig. 4C, Table S7). We then correlated EV-long RNA expression with STIR-positivity across FSHD STIR- and FSHD STIR+ samples, identifying 606 positively and 159 negatively associated long transcripts (Table S8), with the top 10 positively and negatively correlated ones, ranked by p-value, shown in Fig. 5D. As for EV small RNAs, we integrated DEG (Fig. 4A–C) and correlation analysis (Fig. 4D, Table S9) but neither the intersection nor the union provided a set of EV-long RNAs capable of discriminating STIR+ samples from the others. Using a complementary strategy, we then inspected boxplots of each transcript across CTRL, NPGC, FSHD STIR-, and FSHD STIR+ EV groups and selected those showing clear upregulation or downregulation in STIR+ samples compared to the others. This yielded 14 upregulated and 30 downregulated EV-long RNAs, identified as exploratory candidates associated with STIR-positivity (Table S9). Table S10 reports overlap and exclusivity between DEG and correlation results. The combined panel of 14 upregulated EV-long transcripts showed significant separation of FSHD STIR+ samples compared to both FSHD STIR- and NPGC EVs (Fig. 4E). The 30 downregulated EV-long transcripts significantly distinguished FSHD STIR+ samples from FSHD STIR- and CTRL groups (Fig. 4F). The GO BP enrichment analysis suggested that upregulated EV-long RNAs could be involved in pathways related to innate immune response and activation of immune effector processes (Fig. 4G), whereas downregulated EV-long RNAs with T-cell related pathways and transcriptional regulation (Fig. 4G). KEGG analysis suggested that upregulated EV-long RNAs could be associated with pathways related to $CD4^+$ T cell subtype differentiation and Notch signaling (Fig. 4H), whereas downregulated EV-long RNAs with intracellular signal transduction and G-protein coupled receptor signaling (Fig. 4H).

Candidate muscle EV-RNA biomarkers of muscle degeneration

We then compared EV-RNA cargo between FSHD muscles with and without fatty replacement, using T1 signal on MRI at baseline (described in Table 1) as a marker of muscle degeneration. We performed the DEmiR analysis and identified 9 miRNAs significantly dysregulated in EVs from FSHD T1+ muscles compared to FSHD T1- muscles (Fig. 5A, Table S11): 7 were upregulated and 2 downregulated in FSHD T1+ EVs (Fig. 5A, Table S11). The correlation analysis between EV-miRNA expression levels and T1-score (assigned score based on T1 hyperintensity extent; see Methods) identified 7 miRNAs with significant positive and 2 with significant negative correlation to T1-score (Fig. 5B). To establish a muscle EV-miRNA signature associated with T1-positivity, we integrated DemiRs (Fig. 5A, Table S11) and correlation (Fig. 5B) analyses. The union of these two datasets identified 9 upregulated (hsa-mir-134-5p, hsa-mir-181c-5p, hsa-mir-214-3p, hsa-mir-221-3p, hsa-mir-23a-5p*, hsa-mir-369-5p, hsa-mir-92b-3p, hsa-mir-382-5p and hsa-mir-296-3p*) and 3 downregulated (hsa-mir-30a-5p, hsa-mir-590-5p* and hsa-mir-345-5p) EV-miRNAs associated with T1-positivity. In Table S12 are reported the exclusive and/or shared EV-miRNAs across DEmiRs and correlation analyses. The 9 upregulated (Fig. 5C) and 3 downregulated (Fig. 5D) EV-miRNAs significantly separated FSHD T1+ from FSHD T1- samples. The GO BP enrichment analysis suggested that the targets of both upregulated and downregulated miRNAs in FSHD T1+ EVs converged on common set of biological functions (Fig. 5E). These included T cell differentiation, myeloid cell homeostasis, muscle and neural development, somatic diversification of immune receptors, SMAD-mediated signaling, epigenetic regulation

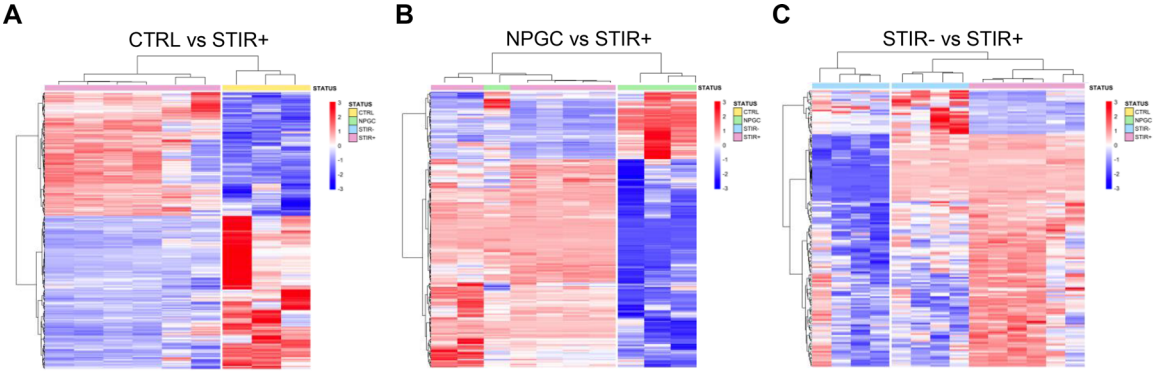

D

	correlation	pvalue	long RNA
STIR-positivity	0,8839	0,00003	ENSG00000200393
	0,8713	0,00005	MIR514A2
	0,8631	0,00007	ENSG00000259702
	0,8613	0,00008	ENSG00000216093
	0,8613	0,00008	ENSG00000222389
	0,8613	0,00008	ENSG00000238591
	0,8613	0,00008	ENSG00000251871
	0,8613	0,00008	ENSG00000252200
	0,8593	0,00008	IL24
	0,8593	0,00008	GRASLND
	-0,8603	0,00008	KLF2
	-0,8603	0,00008	ENSG00000180189
	-0,8603	0,00008	CFD
	0,8603	0,00008	CERS6.AS1
	-0,8593	0,00008	KLF6
	-0,8593	0,00008	CDC42
	-0,8593	0,00008	YPEL5
	-0,8593	0,00008	RPS27A
	-0,8593	0,00008	CTNNB1
	-0,8593	0,00008	PTP4A2

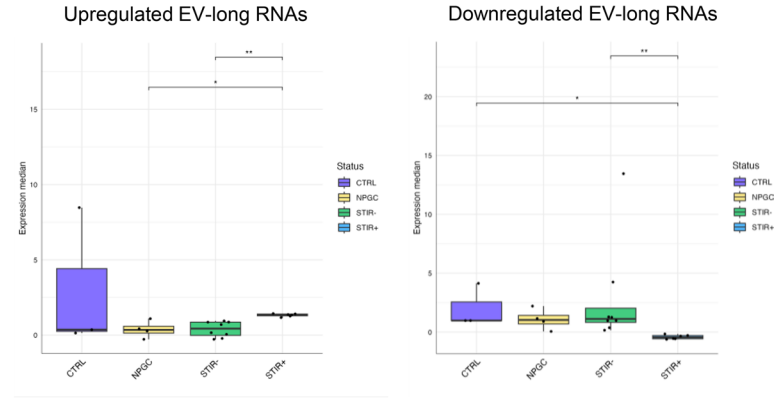

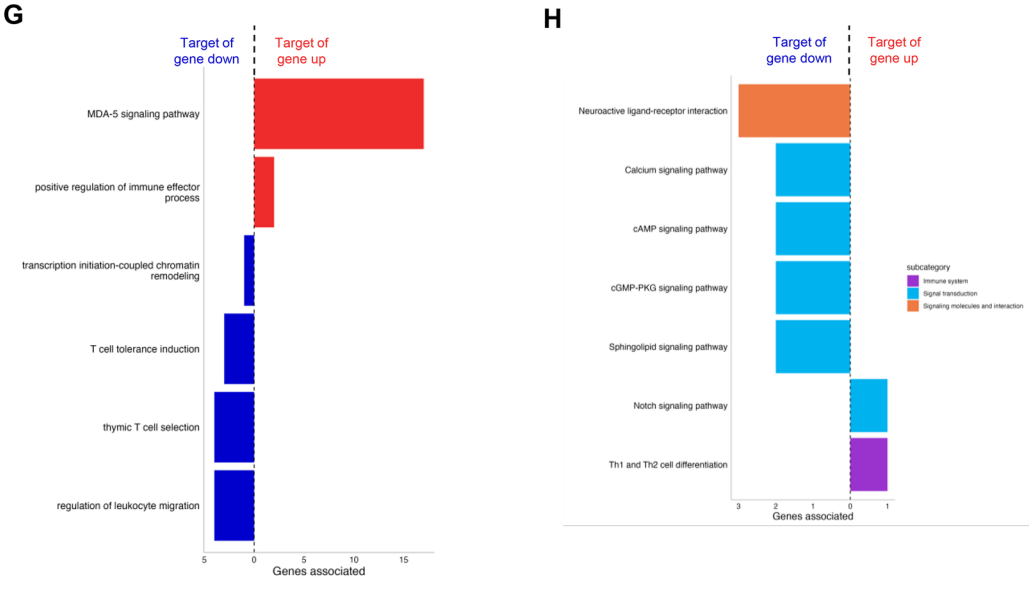

Fig. 4 Muscle EV-long transcript signature in FSHD STIR+ muscles. Heatmaps of differentially expressed long transcripts between FSHD STIR+ ($n=6$) and CTRL ($n=3$) (**A**), NPGC ($n=3$) (**B**), or FSHD STIR− ($n=8$) (**C**). (**D**) top 10 EV-long transcripts positively and negatively correlated with STIR-positivity [Spearman's correlation coefficient (correlation) and p-value reported]. (E–F) boxplots of 4 upregulated (**E**) and 30 downregulated (**F**) EV-long transcripts; each dot represents the median expression of selected genes per sample. Groups were compared using the Kruskal–Wallis with Dunn's post hoc test; (* $p<0.05$; ** $p<0.01$). (G–H) GO BP (**G**) and KEGG (**H**) enrichment analyses of upregulated (red) and downregulated (blue) EV-long RNA biomarkers. Bar lengths indicate the relative number of genes associated with each biological process or pathway

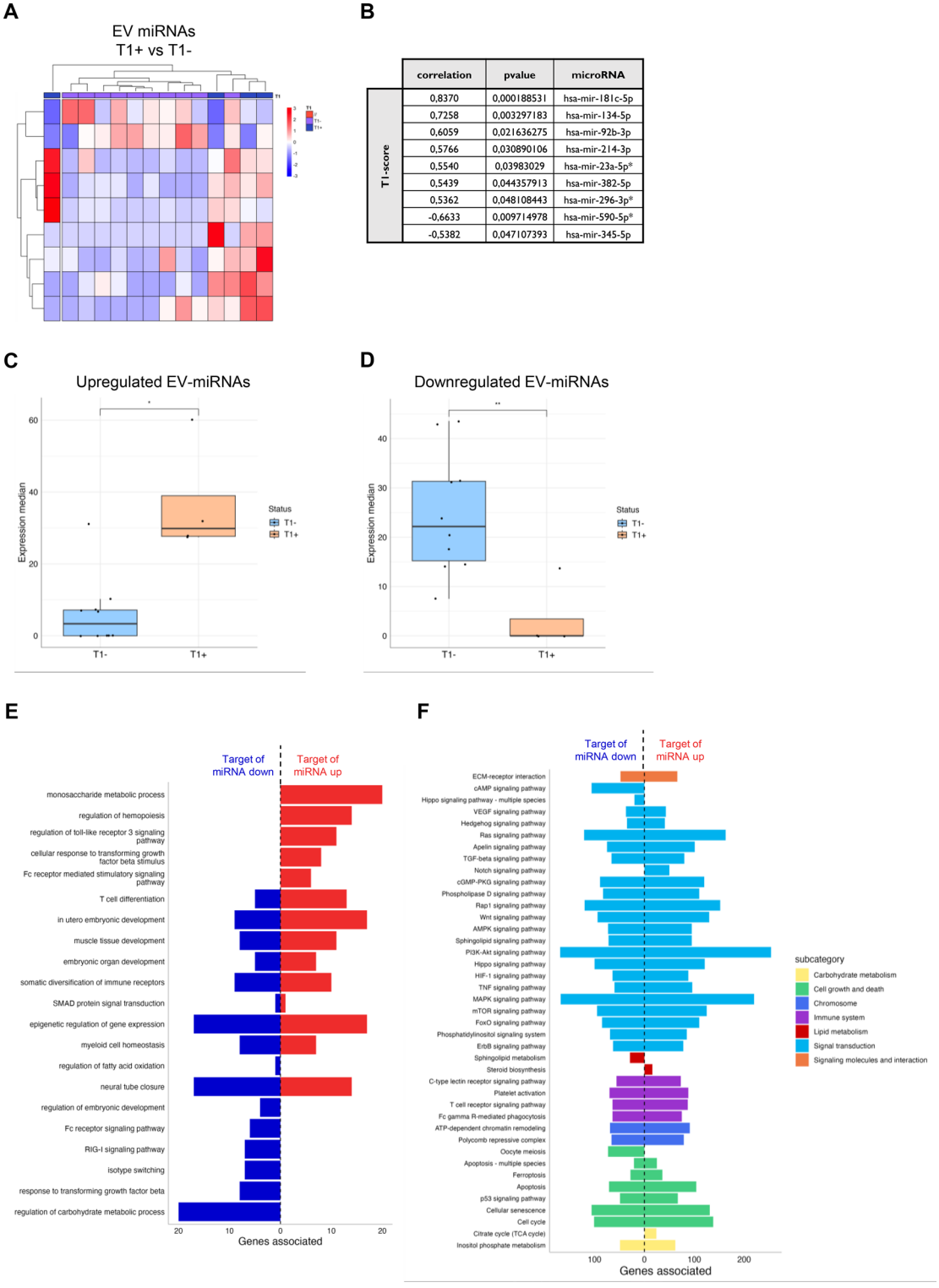

Fig. 5 Muscle EV-miRNA signature in FSHD T1+ muscles. Heatmap of differentially expressed miRNAs between FSHD T1+ ($n=4$) and T1− ($n=10$) (**A**). (**B**) EV-miRnas significantly correlated with T1-score (Spearman's correlation coefficient and p-values shown). (C–D) boxplots of 9 upregulated (**C**) and 3 downregulated (**D**) EV-miRNAs; each dot represents median expression of selected miRNAs per sample. (E–F) GO BP (**E**) and KEGG (**F**) enrichment analyses of upregulated (red) and downregulated (blue) EV-miRNA biomarkers. Bar lengths indicate the relative number of predicted target genes associated with each biological process or pathway. Groups were compared using the Wilcoxon signed-rank test (* $p<0.05$; ** $p<0.01$)

of gene expression, and both fatty acid and carbohydrate metabolism (Fig. 5E). Similarly, KEGG pathway enrichment analysis suggested shared involvement in core signaling cascades such as intracellular signaling, immune response, apoptosis, cell cycle regulation, epigenetic control, lipid metabolism, and extracellular matrix organization (Fig. 5F). Then, we profiled isomiR cargo in EVs from FSHD T1+ and T1- muscles. The comparative boxplot analysis revealed no statistically significant differences in nucleotide modifications between the two groups (Fig. S3). The DEisomiR analysis showed that 32 isomiRs were significantly dysregulated in FSHD T1+ EVs compared to T1- EVs, of whom 30 were upregulated and 2 downregulated (Fig. 6A, Table S13). The correlation analysis between EV-isomiR expression levels and T1-score identified 50 isomiRs with significant positive and 5 with significant negative correlation to T1-score (Table S14). The top 10 positively correlated EV-isomiRs, ranked by p-value, are shown in Fig. 6B, along with the 5 negatively correlated ones (Fig. 6B). To establish a muscle EV-isomiR signature associated with T1-positivity, we integrated DEisomiRs (Fig. 6A, Table S13) and correlation (Fig. 6B, Table S14) analyses. The union of these two datasets identified 62 upregulated and 7 downregulated

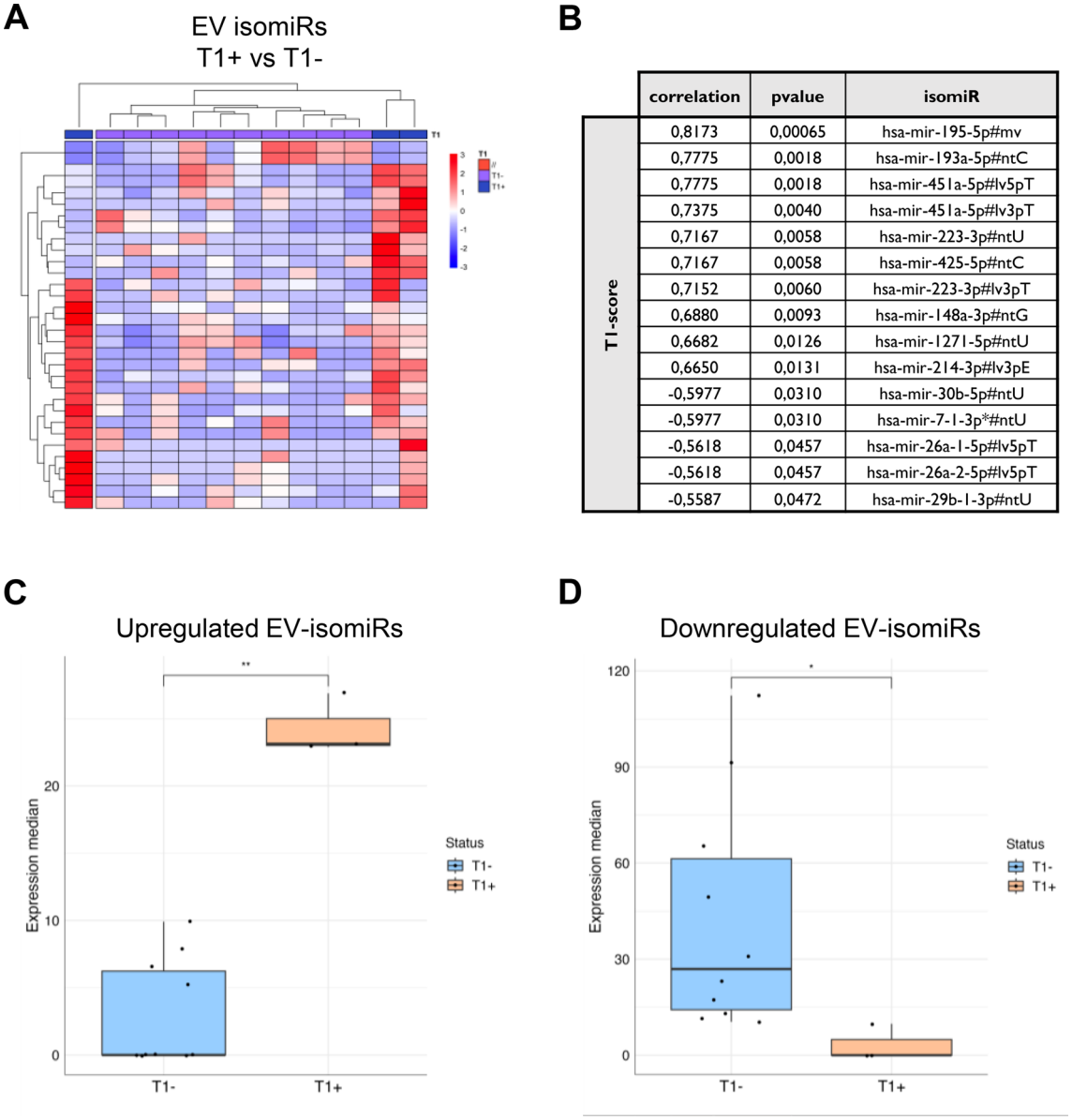

	correlation	pvalue	isomiR
T1-score	0,8173	0,00065	hsa-mir-195-5p#mv
	0,7775	0,0018	hsa-mir-193a-5p#ntC
	0,7775	0,0018	hsa-mir-451a-5p#lv5pT
	0,7375	0,0040	hsa-mir-451a-5p#lv3pT
	0,7167	0,0058	hsa-mir-223-3p#ntU
	0,7167	0,0058	hsa-mir-425-5p#ntC
	0,7152	0,0060	hsa-mir-223-3p#lv3pT
	0,6880	0,0093	hsa-mir-148a-3p#ntG
	0,6682	0,0126	hsa-mir-1271-5p#ntU
	0,6650	0,0131	hsa-mir-214-3p#lv3pE
	-0,5977	0,0310	hsa-mir-30b-5p#ntU
	-0,5977	0,0310	hsa-mir-7-1-3p*#ntU
	-0,5618	0,0457	hsa-mir-26a-1-5p#lv5pT
	-0,5618	0,0457	hsa-mir-26a-2-5p#lv5pT
	-0,5587	0,0472	hsa-mir-29b-1-3p#ntU

Fig. 6 Muscle EV-isomiR signature in FSHD T1+ muscles. Heatmap of differentially expressed isomiRs between FSHD T1+ ($n=3$) and T1− ($n=10$) (**A**). (**B**) top 10 positively and 5 negatively T1-score–correlated EV-isomiRs (Spearman's correlation coefficient and p-values shown). (C-D) boxplots of 62 upregulated (**C**) and 7 downregulated (**D**) EV-isomiRs; each dot represents the median expression of selected isomiRs per sample. Groups were compared using the Wilcoxon signed-rank test (* $p<0.05$; ** $p<0.01$)

EV-isomiRs associated with T1-positivity (Table S15). In Table S16 are reported the exclusive and/or shared EV-isomiRs across DEisomiRs and correlation analyses. The 62 upregulated (Fig. 6C) and 7 downregulated (Fig. 6D) EV-isomiRs significantly separated FSHD T1+ from FSHD T1- samples. Finally, we investigated the long RNA cargo of EVs in relation to the T1-positivity of FSHD muscles. The DEG analysis identified 192 long RNAs significantly dysregulated in FSHD T1+ EV samples compared to FSHD T1- EVs (Fig. 7A, Table S17). Specifically, 124 long RNAs were upregulated and 68 downregulated in FSHD T1+ compared to FSHD T1- (Fig. 7A, Table S17). The correlation analysis between EV-long RNA expression levels and T1-score identified 732 long RNAs with significant positive and 464 with significant negative correlation to T1-score (Table S18). The top 10 positively and negatively correlated EV-long RNAs, ranked by p-value, are shown in Fig. 7B. As for EV-long RNAs and STIR-positivity, we had to select transcripts displaying specific upregulation or downregulation in EVs from FSHD T1+ muscles compared to FSHD T1- samples, considering them as exploratory candidates. This analysis resulted in a list of 27 upregulated and 5 downregulated EV-long RNAs associated with T1-positivity (Table S19). In Table S20 are reported the exclusive and/or shared EV-long RNAs across DEG and correlation analyses. The 27 upregulated (Fig. 7C) and 5 downregulated (Fig. 7D) EV-long RNAs significantly separated FSHD T1+ from FSHD T1- samples. The GO BP enrichment analysis suggested that the 27 upregulated EV-long RNAs in FSHD T1+ EVs could be involved in pathways related to innate immunity, development and carbohydrate metabolism (Fig. 7E). KEGG pathway enrichment analysis suggested their involvement in pathways related to cell signal transduction and carbohydrate metabolism (Fig. 7F). Both enrichment analyses did not reveal any significant pathways linked to the 5 downregulated EV-long RNAs.

Candidate muscle EV-RNA biomarkers and disease progression

We explored whether EV-associated RNA signatures, previously linked to STIR-positivity [miRNAs (Fig. 2E–F), isomiRs (Fig. 3G–H; Table S5), long RNAs (Fig. 4E–F; Table S9)] and T1-positivity [miRNAs (Fig. 5C–D), isomiRs (Fig. 5I–J; Table S15), long RNAs (Fig. 6C–D; Table S19)], showed association to longitudinal disease progression. Disease progression was defined by an increase in the T1-score on MRI scans between baseline and the 2-year MRI follow-up (17/22 muscles). Therefore, FSHD patients' muscles were stratified retrospectively into "yes" or "no" progression (Table 1). Both EV-miRNAs and EV-isomiRs upregulated in STIR+ muscle-derived EVs were significantly upregulated in FSHD muscles that progressed compared to those that remained stable over the 2-year MRI follow-up (Fig. 8A–B). A similar trend emerged for EV-long RNAs: both those upregulated and downregulated in STIR+ EVs showed significant different expression at baseline between "no progression" and "progression" groups (Fig. 8C–D). In contrast, among the candidate EV biomarkers previously associated with muscle degeneration (T1+ vs. T1–), only the downregulated EV-long RNAs in FSHD T1+ samples were significantly upregulated in muscles that progressed compared to those that did not (Fig. 8E). Boxplots showing non-significant differences across groups are available in Supplementary Fig. S4.

Discussion

In the present exploratory study, we provide a comprehensive analysis of RNA cargo from skeletal muscle-derived EVs, profiling small and long RNAs from ex-vivo tissue culture of MRI-characterized muscles of FSHD patients. We identified EV-RNA signatures associated with both disease activity (i.e. STIR+ muscles) and muscle degeneration (i.e. T1+ muscles). The small RNA profiling revealed that the global distribution of RNA classes was not different among CTRL, NPGC, STIR-and STIR+ EVs, while specific miRNAs and isomiRs were selectively dysregulated in STIR+ samples. This could suggest that disease activity does not alter overall small RNA classes but specifically modulates individual RNA species. The EV-miRNA signature we identified not only was characteristic of STIR+ EVs compared to STIR-, NPGC, and CTRL samples but showed also enrichment in pathways relevant for FSHD. [5, 18,21]. Notably, miR-382-5p (up in STIR+ EVs) is upregulated in FSHD myoblasts compared to healthy controls and other dystrophic samples [47], miR-146b-5p (up in STIR+ EVs) is increased in the plasma of FSHD patients [29], and serves as serum inflammatory marker in bowel disease. [48] Likewise, miR-146a-5p (up in STIR+ EVs) is upregulated in Duchenne muscular dystrophy (DMD) biopsies [49], and in the sera of patients with inflammatory myopathies. [48, 50, 51] MiR-409-3p (up in STIR+ EVs) is elevated in DMD muscles [52], whereas miR-16–2-5p (down in STIR+ EVs) is downregulated in inclusion body myositis. [53] MiR-337-3p (up in STIR+ EVs) [54], and miR-27b-3p (down in STIR+ EVs) [55, 56] have been implicated in the positive and negative regulation of muscle adipogenesis, fibrosis, and atrophy, respectively. Collectively, these data reinforce that EV-miRNAs from STIR+ muscles mirror both inflammatory and early degenerative processes in FSHD, underscoring their mechanistic relevance in disease activity, and supporting their potential for clinical translation. The small RNA-seq analysis also enabled us to profile isomiRs, sequence variants of canonical miRNAs generated by alternative Dicer/Drosha cleavage and post-transcriptional nucleotide modifications. [57] Depending

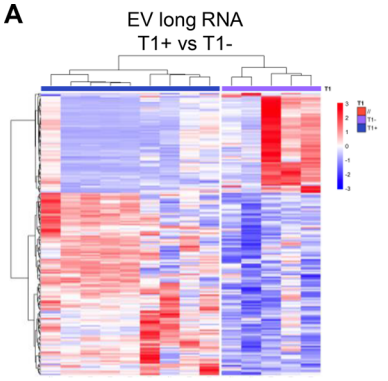

B

	correlation	pvalue	long RNA
T1-score	0,8152	0,00038	SNORD115.41
	0,8152	0,0004	ENSG00000221409
	0,8152	0,0004	ENSG00000255637
	0,8152	0,0004	ENSG00000255972
	0,7990	0,0006	ENSG00000237133
	0,7990	0,0006	ENSG00000238051
	0,7978	0,0006	ENSG00000201153
	0,7907	0,0008	C19orf33
	0,7907	0,0008	ENSG00000198082
	0,7907	0,0008	DEFB107A.1
	-0,9042	0,0000	CCDC88B
	-0,8635	0,0001	SGSM2
	-0,8617	0,0001	GPC1
	-0,8579	0,0001	KDM4B
	-0,8571	0,0001	THAP11
	-0,8533	0,0001	ITGB5
	-0,8496	0,0001	STK35
	-0,8450	0,0001	RNU6ATAC
	-0,8441	0,0001	IRF2BP1
	-0,8440	0,0001	CRKL

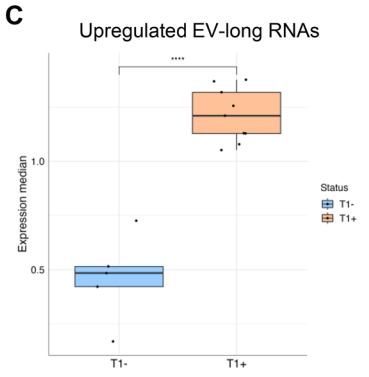

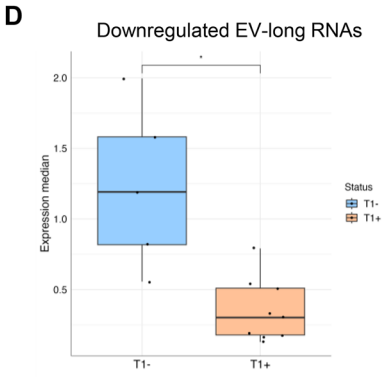

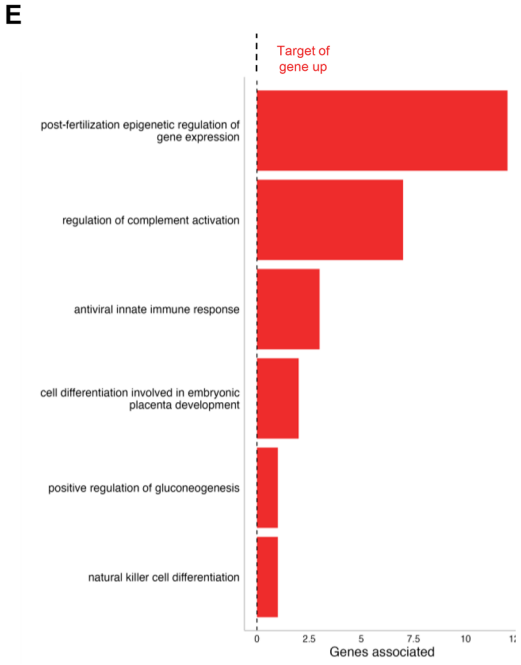

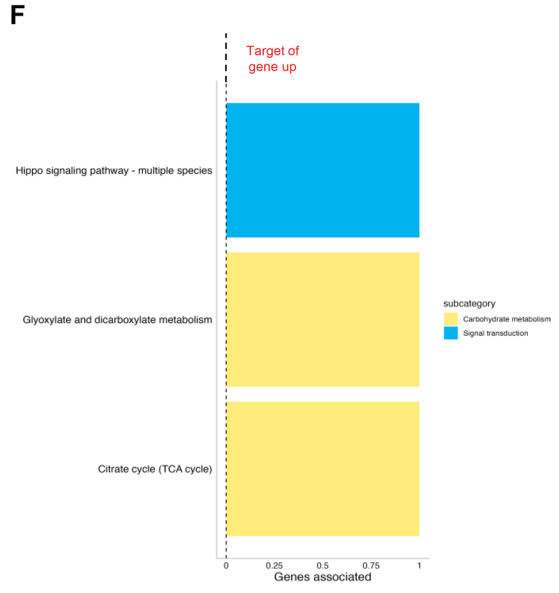

Fig. 7 Muscle EV-long RNA signature in FSHD T1+ muscles. Heatmap of differentially expressed long RNAs between FSHD T1+ ($n=4$) and T1− ($n=10$) (**A**). (**B**) top 10 EV-long transcripts positively and negatively correlated with STIR-positivity [Spearman's correlation coefficient (correlation) and p-value reported]. (C–D) boxplots of 27 upregulated (**C**) and 5 downregulated (**D**) EV-long RNAs; each dot represents the median expression of selected genes per sample. (E–F) GO BP (**E**) and KEGG (**F**) enrichment analyses of upregulated (red) EV-long RNA biomarkers. Bar lengths indicate the relative number of genes associated with each biological process or pathway. Groups were compared using the Student's t-test (* $p<0.05$; **** $p<0.0001$)

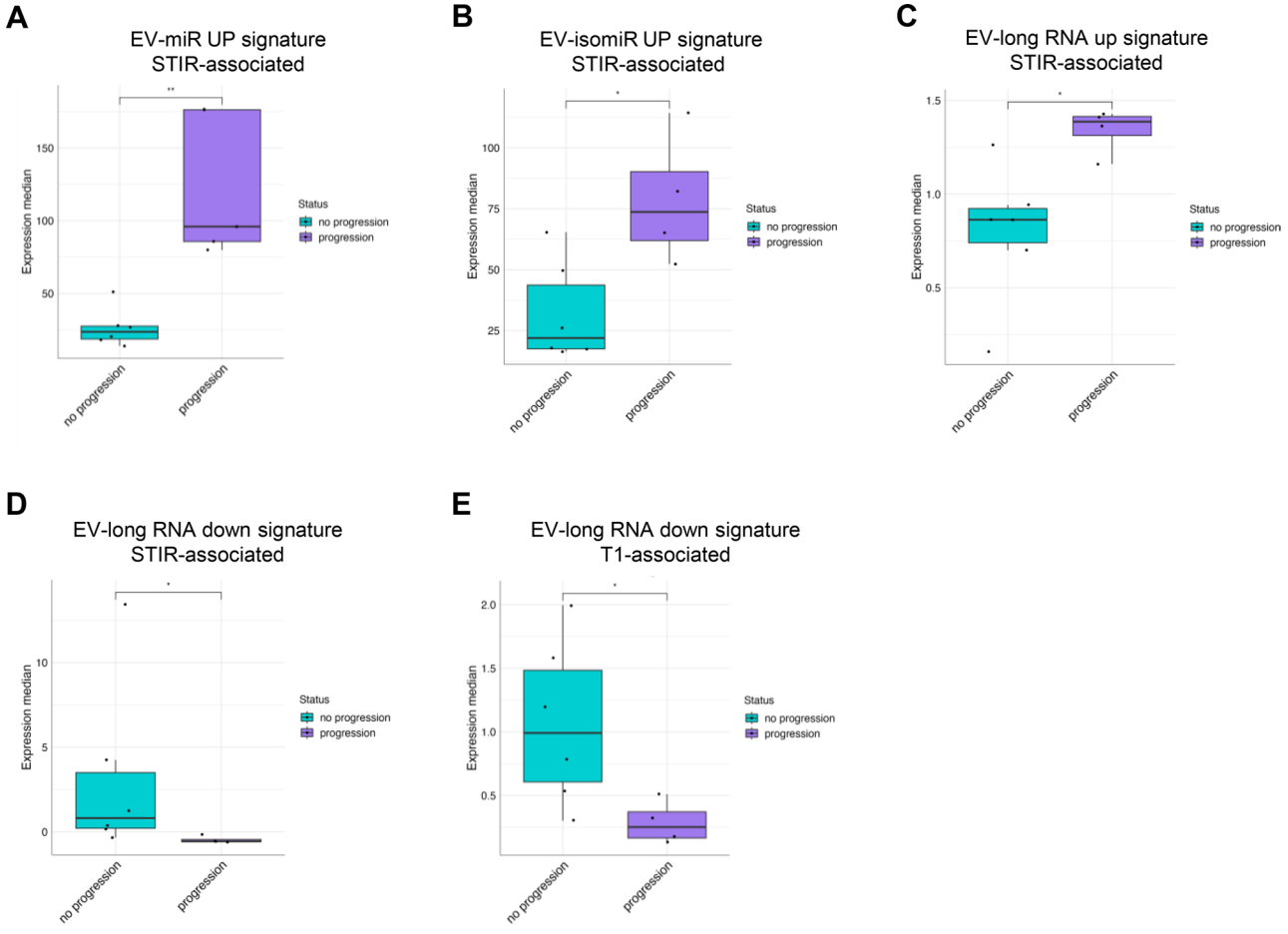

Fig. 8 Baseline expression of EV-RNA biomarkers and disease progression. Boxplots show the expression levels of candidate EV-miRNAs (**A**), EV-isomiRs (**B**), and EV-long transcripts (**C**–**D**) associated with STIR-positivity, as well as EV-long RNAs (**E**) linked to T1-positivity. Data refer to baseline expression in FSHD muscle–derived EVs from samples that did or did not show T1-score changes at the 2-year MRI follow-up. Each dot represents the median expression of selected EV-RNA biomarkers per sample. Groups were compared using unpaired two-tailed Student's t-test (assuming equal or unequal variances) or Wilcoxon rank-sum test, based on data distribution and variance homogeneity assessed by Shapiro–Wilk and Levene's tests (* $p < 0.05$; ** $p < 0.01$)

on the specific alteration, an isomiR can share or diverge from its parent miRNA in target specificity and functional impact. Although their precise biological roles remain under active investigation, a growing body of work highlights isomiRs as promising diagnostic and prognostic biomarkers. [57] We interestingly found distinct miRNA processing signatures in NPGC muscle EVs: ntU events uniquely distinguish NPGC from CTRL whereas mv events separate NPGC from CTRL and STIR- muscles. The uridylation modification is a well described post transcriptional modification that can influence miRNA stability, turnover, and target selection. Indeed, 3′ uridylation events have been reported across multiple tissues and disease contexts and are thought to reflect regulated steps in miRNA maturation and decay. [58] Mv isomiRs instead can carry more than one simultaneous modification, such as trimming, shifting, or non templated additions, indicating a broader heterogeneity in miRNA processing. [59] These alterations may reflect dysregulation of RNA editing or terminal modification enzymes such as terminal uridylyl transferases (TUTases) [60], and may be worth investigating their potential role in modulating processes underlying the incomplete penetrance of FSHD. We next identified exploratory EV-long RNA signatures associated to STIR+ EVs. Among them, several genes with key roles in muscle physiology and immune regulation emerged. *Ankyrin repeat domain-containing protein 17 (ANKRD17)* (up in STIR+ EVs) positively regulates innate immunity [61], *Nuclear receptor coactivator 6 (NCOA6)* (up in STIR+ EVs) and *ENSG00000143466* (down in STIR+ EVs) appear to positively and negatively regulate the NLRP3 inflammasome [62, 63], respectively. *Protein tyrosine phosphatase receptor type J (PTPRJ)* (up in STIR+ EVs) is expressed in activated T lymphocytes and memory B cells [64], whereas *Adenosine A1 receptor (ADORA1),* [65] and *DM1 antisense transcript (DM1-AS),* [66] both downregulated in STIR+ EVs, are implicated in myotonic dystrophy type 1

(*DM1*) pathogenesis. Loss of function mutations of *Autoimmune regulator (AIRE)* (down in STIR+ EVs) are associated with a progressive limb-girdle-like autoimmune myopathy. [67] Building on the findings from EV-based STIR+ biomarker analysis, we next investigated the molecular signatures associated with T1-positive MRI signal, as a sign of muscle degeneration. We identified panels of EV-miRNAs enriched in EVs from T1+ muscles compared to EVs from T1- ones. These EV-miRNAs seem to participate in known muscle-damage pathways. For example, miR-181c-5p [68], and miR-23a-5p [69] are both positively related to muscle atrophy and are upregulated in T1+ EVs. MiR-214-3p [70] and miR-382-5p [71], both upregulated in T1+ EVs, positively regulate muscle fibrosis and degeneration in DMD muscles. In contrast, miR-30a-5p (down in T1+ EVs) has been reported to exert negative regulation on these pathological processes. [72] MiR-221-3p [73] and miR-92b-3p [74], both upregulated in T1+ EVs, positively affect adipogenesis. This pattern suggests that EV-miRNA profiles reflect the key molecular events driving muscle degeneration in FSHD. Subsequently, we identified panels of EV-isomiRs significantly dysregulated in T1+ muscles, but unlike EVs derived from NPGC muscles, muscle degeneration does not appear to trigger new canonical miRNA editing events. Finally, we found exploratory EV-long RNA signatures associated with T1-positivity of muscles. Among them, several transcripts are functionally linked to adipogenic remodelling and skeletal muscle plasticity. *ABI family member 3 binding protein (ABI3BP)* (up in T1+ EVs) is involved in the differentiation of mesenchymal stem cells into adipocytes [75], while *Cysteine-rich secretory protein LCCL domain-containing 2 (CRISPLD2)* (up in T1+ EVs) acts as an adipokine to regulate adipose tissue remodeling. [76] Key positive regulators of adipogenesis include *DNA damage-binding protein 1 (DDB1),* [77] *Family with sequence similarity 13 member A (FAM13A),* [78] and *Zinc finger protein 423 (ZNF423),* [79] null *Early B-cell factor 1 (EBF1),* [80] and *EH domain-binding protein 1 (EHBP1),* [81] all upregulated in T1+ EVs. Other candidate transcripts, including *PR/SET domain 2 (PRDM2) and Sushi, von Willebrand factor type A, EGF and pentraxin domain-containing 1 (SVEP1),* [82, 83] both up in T1+ EVs, are involved in the impairment of skeletal muscle plasticity and regenerative potential. We thus explored whether the expression levels of our candidate EV-RNAs at baseline, linked to disease activity and muscle degeneration, could show association with muscles that progressed compared with those that remained stable over 2-years. EV-miRNAs and EV-isomiRs upregulated in STIR-positive samples, as well as both up- and down-regulated EV-long RNAs in STIR+ EVs, showed differential expression between progressive and stable muscles. Furthermore, the EV-long RNAs downregulated in T1-positive muscles displayed only modest signals of discrimination. This likely reflects that STIR-positivity marks an active, pre-degenerative inflammatory phase, whereas T1-positivity corresponds to a chronic fatty replacement process. Methodological limitations of this study include the small sample size and the use of short-term muscle explant cultures for EV isolation. The limited cohort, inherent to the rarity of the disease and the challenges associated with obtaining fresh muscle biopsies, supports interpreting these findings as an exploratory discovery study. The explant approach, although enhancing tissue specificity and increasing RNA yield, may introduce ex-vivo artifacts by influencing EV secretion profiles, which may not fully recapitulate native tissue physiology. [84] In addition, the kit-based EV isolation method, while practical for low-input samples, may capture mixed vesicle populations or co-isolated non-vesicular material, a known limitation of precipitation-based approaches. Nonetheless, by ensuring that EVs originate from muscles with specific MRI features, the explant model offers a unique opportunity to anchor molecular data to localized disease activity. These EV-based molecular signatures, leveraging the stability and selective packaging of EV cargo, may also be detectable in circulation. Prior work in other neuromuscular disorders supports the feasibility of EV-RNA transferability between tissues and blood. [85] Future studies should validate the translational relevance of these EV-RNA signatures for disease monitoring and progression in circulation, in larger and independent cohorts, and additionally investigate their functional roles in FSHD pathogenesis, including mechanistic studies and functional assays for the most promising candidate EV-RNAs.

Conclusions

For the first time, we provide an RNA profiling of muscle-derived EVs in FSHD, revealing candidate biomarkers that mirror both disease activity and muscle degeneration. Our findings support the investigation of muscle-EV RNAs as a potential non-invasive liquid biopsy approach for FSHD, with further validation needed to assess their complementarity to MRI for patient stratification and therapeutic monitoring in clinical trials.

Abbreviations

FSHD	Facioscapulohumeral muscular dystrophy
EVs	Extracellular vesicles
NPGC	Non-penetrant gene carriers
MRI	Magnetic resonance imaging
T1	T1-weighted sequences
STIR	Short-tau inversion recovery sequences
STIR+	STIR-positive
STIR-	STIR-negative
CTRL	Healthy controls
NTA	Nanoparticle Tracking Analysis
DEmiR	Differentially expressed miR
DEisomiR	Differentially expressed isomiR

DEG	Differentially expressed gene
miRNAs	microRNAs
GO BP	Gene Ontology Biological Process
KEGG	Kyoto Encyclopedia of Genes and Genomes
NtU	Non-template uridylation
Mv	Multiple variant
NtC	Non-template cytosine addition
NtG	Non-template guanine addition
Lv5pE	Leading variant 5′extension
LvepE	Leading variant end processing extension
Lv3pT	Leading variant 3′trimming

Supplementary Information

The online version contains supplementary material available at https://doi.org/10.1186/s12967-026-07794-y.

Supplementary Material 1

Supplementary Material 2

Acknowledgements
We are extremely grateful to the FSHD Italia Onlus association, the patients and their families for their constant support. We would like to acknowledge the valuable support of Preanalytical and Cell Biology, Multispecialistic Biobank, Microscopy, Single Cell, Genomics and Bioinformatic Core Facilities of Gemelli Science and Technology Park (G-STeP) of the Fondazione Policlinico Universitario "A. Gemelli" IRCCS for sample processing and analysis. We also gratefully acknowledge the Regenerative Medicine Research Center (CROME) of the Università Cattolica del Sacro Cuore for their scientific contribution and collaboration.

Authors' contributions
Conceptualization: ERagozzino, ER, LDP, AP, OP. Methodology: ERagozzino, SN, AT, VN, DS, GK, FV, AS, MP, VS, AA, DL, AS. Data analysis: ERagozzino, EO, LDP, AP, LG, GM, OP. Clinical investigation: SB, ET, MM, BR, GT, ER. Writing original draft: ERagozzino, LDP, AP. Writing review and editing: ERagozzino, LDP, AP, WL, OP, ER. All authors read and approved the final manuscript.

Funding
This study was supported by SOLVE FSHD and by Next Generation EU Ministero dell'Università e della Ricerca Grant number PRIN2022_2022ALH2Z8_LS2 Cup: J53D23003070008 to ERicci. E.Ragozzino was supported by 3-year fellowship by Centro Universitario Cattolico, promoted by Conferenza Episcopale Italiana.

Data availability
The RNA-sequencing datasets generated in this study are available from the corresponding author upon reasonable request and following approval by the institutional Data Protection Officer. Researchers requesting access should provide a brief description of the intended use, including the scientific purpose and the data protection measures to be implemented.

Declarations

Ethics approval
The protocol was approved on 9 May 2023 by the Etich committee of Fondazione Policlinico Universitario A.Gemelli and Università Cattolica del Sacro Cuore of Rome (protocol ID 4973).

Consent for publication
Not applicable

Competing interests
The authors declare that they have no competing interests.

Author details
[1]Dipartimento di Scienze della Vita e Sanità Pubblica, Università Cattolica del Sacro Cuore, Largo Francesco Vito 1, 00168 Rome, Italy
[2]Unità Operativa Complessa di Neurologia, Fondazione Policlinico Universitario A. Gemelli IRCCS, 00168 Rome, Italy
[3]Fondazione Policlinico Universitario A. Gemelli IRCCS, 00168 Rome, Italy
[4]Bioinformatics Facility Core Research, Gemelli Science and Technology Park (GSTeP) Fondazione Policlinico Universitario A. Gemelli IRCCS, 00168 Rome, Italy
[5]Dipartimento di Medicina e Chirurgia Traslazionale, Università Cattolica del Sacro Cuore, 00168 Rome, Italy
[6]Istituto Telethon di Genetica e Medicina, 80078 Pozzuoli, Italy
[7]Dipartimento di Medicina di Precisione, Università della Campania "Luigi Vanvitelli", 80138 Naples, Italy
[8]Dipartimento di Neuroscienze, Università Cattolica del Sacro Cuore, 00168 Rome, Italy
[9]Multiplex Spatial Profiling Facility, Gemelli Science and Technology Park (GSTeP) Fondazione Policlinico Universitario A. Gemelli IRCCS, 00168 Rome, Italy
[10]John Walton Muscular Dystrophy Research Centre, Newcastle University and Newcastle Hospitals NHS Foundation Trusts, Newcastle Upon Tyne, UK
[11]Fondazione IRCCS Casa Sollievo della Sofferenza, San Giovanni Rotondo 71013, Foggia, Italy

Received: 15 September 2025 / Accepted: 25 January 2026
Published online: 25 February 2026

References

1. Shatzl T, Kaiser L, Deigner HP. Facioscapulohumeral muscular dystrophy: genetics, gene activation and downstream signalling with regard to recent therapeutic approaches: an update. Orphanet J Rare Dis. 2021, Mar, 12;16(1):129
2. Xie Q, Ma G, Song Y. Therapeutic strategy and clinical path of facioscapulohumeral muscular dystrophy: review of the current literature. Appl Sci. 2024;14(18):8222
3. Statland JM, Tawil R. Risk of functional impairment in facioscapulohumeral muscular dystrophy. Muscle Nerve. 2014;49:520–27
4. Wang ZQ, Wang N, van der Maarel S, Murong SX, Wu ZY. Distinguishing the 4qA and 4qB variants is essential for the diagnosis of facioscapulohumeral muscular dystrophy in the Chinese population. Eur J Hum Genet. 2011, Jan;19(1):64–69
5. Tihaya MS, Mul K, Balog J, et al. Facioscapulohumeral muscular dystrophy: the road to targeted therapies. Nat Rev Neurol. 2023, Feb;19(2):91–108
6. Monforte M, Bortolani S, Torchia E, et al. Diagnostic magnetic resonance imaging biomarkers for facioscapulohumeral muscular dystrophy identified by machine learning. J Neurol. 2022, Apr;269(4):2055–63
7. Monforte M, Attarian S, Vissing J, Diaz-Manera J, Tasca G. 265th ENMC workshop participants. 265th ENMC International workshop: muscle imaging in facioscapulohumeral muscular dystrophy (FSHD): relevance for clinical trials. 22–24 April 2022, Hoofddorp, the Netherlands. Neuromuscul Disord. 2023, Jan;33(1):65–75
8. Paoletti M, Monforte M, Barzaghi L, et al. Natural history of facioscapulohumeral muscular dystrophy evaluated by multiparametric quantitative MRI: a prospective cohort study. J Neurol. 2025, Apr, 2;272(4):306
9. Vincenten SCC, Teeselink S, Mul K, et al. Muscle imaging in facioscapulohumeral muscular dystrophy research: a scoping review and expert recommendations. Neuromuscul Disord. 2025, Feb;47:105274
10. Tasca G, Monforte M, Iannaccone E, et al. Upper girdle imaging in facioscapulohumeral muscular dystrophy. PLoS One. 2014, Jun, 16;9(6):e100292
11. Tasca G, Monforte M, Ottaviani P, et al. Magnetic resonance imaging in a large cohort of facioscapulohumeral muscular dystrophy patients: pattern refinement and implications for clinical trials. Ann Neurol. 2016, May;79(5):854–64
12. Warman-Chardon J, Diaz-Manera J, Tasca G, Straub V. 247th ENMC International workshop: muscle magnetic resonance imaging - implementing muscle MRI as a diagnostic tool for rare genetic myopathy cohorts. Hoofddorp, the Netherlands, September 2019. Neuromuscul Disord. 2020 Nov;30(11):938–47
13. Tasca G, Pescatori M, Monforte M, et al. Different molecular signatures in magnetic resonance imaging-staged facioscapulohumeral muscular dystrophy muscles. PLoS One. 2012;7(6):e38779
14. Monforte M, Laschena F, Ottaviani P, et al. Tracking muscle wasting and disease activity in facioscapulohumeral muscular dystrophy by qualitative longitudinal imaging. J Cachexia, Sarcopenia Muscle. 2019;10(6):1258–65

15. Dahlqvist JR, Poulsen NS, Østergaard ST, et al. Evaluation of inflammatory lesions over 2 years in facioscapulohumeral muscular dystrophy. Neurology. 2020, Sep, 1;95(9):e1211–e 1221
16. Dahlqvist JR, Andersen G, Khawajazada T, Vissing C, Thomsen C, Vissing J. Relationship between muscle inflammation and fat replacement assessed by MRI in facioscapulohumeral muscular dystrophy. J Neurol. 2019;266(5):1127–35
17. Frisullo G, Frusciante R, Nociti V, et al. CD8(+) T cells in facioscapulohumeral muscular dystrophy patients with inflammatory features at muscle MRI. J Clin Immunol. 2011, Apr;31(2):155–66
18. Ragozzino E, Bortolani S, Di Pietro L, et al. Muscle fibrosis as a prognostic biomarker in facioscapulohumeral muscular dystrophy: a retrospective cohort study. Acta Neuropathol Commun. 2023, 17;11(1):165
19. Di Pietro L, Giacalone F, Ragozzino E, et al. Non-myogenic mesenchymal cells contribute to muscle degeneration in facioscapulohumeral muscular dystrophy patients. Cell Death Dis. 2022, Sep, 16;13(9):793
20. Wang LH, Friedman SD, Shaw D, et al. MRI-informed muscle biopsies correlate MRI with pathology and DUX4 target gene expression in FSHD. Hum Mol Genet. 2019, Feb, 1;28(3):476–86
21. Wong CJ, Wang LH, Friedman SD, et al. Longitudinal measures of RNA expression and disease activity in FSHD muscle biopsies. Hum Mol Genet. 2020, Apr, 15;29(6):1030–43
22. Tasca G, Monforte M, Corbi M, et al. Muscle microdialysis to investigate inflammatory biomarkers in facioscapulohumeral muscular dystrophy. Mol Neurobiol. 2018, Apr;55(4):2959–66
23. Corasolla Carregari V, Monforte M, Di Maio G, et al. Proteomics of muscle microdialysates identifies potential circulating biomarkers in facioscapulohumeral muscular dystrophy. Int J Mol Sci. 2020, Dec, 30;22(1):290
24. Statland J, Donlin-Smith CM, Tapscott SJ, van der Maarel S, Tawil R. Multiplex screen of serum biomarkers in facioscapulohumeral muscular dystrophy. J Neuromuscul Dis. 2014;1(2):181–90
25. Yao Z, Snider L, Balog J, et al. DUX4-induced gene expression is the major molecular signature in FSHD skeletal muscle. Hum Mol Genet. 2014, 15;23(20):5342–52
26. Petek Lm Rickard AM, Budech C, Poliachik SL, et al. A cross sectional study of two independent cohorts identifies serum biomarkers for facioscapulohumeral muscular dystrophy (FSHD). Neuromuscul Disord. 2016;26(7):405–13
27. Banerji CRS, Zammit PS. PAX7 target gene repression is a superior FSHD biomarker than DUX4 target gene activation, associating with pathological severity and identifying FSHD at the single-cell level. Hum Mol Genet. 2019;28(13)
28. van den Heuvel A, Mahfouz A, Kloet SL, et al. Single-cell RNA sequencing in facioscapulohumeral muscular dystrophy disease etiology and development. Hum Mol Genet. 2019;28(7):1064–75
29. Heier CR, Zhang A, Nguyen NY, et al. Multi-Omics Identifies circulating miRNA and protein biomarkers for facioscapulohumeral dystrophy. J Pers Med. 2020, Nov, 19;10(4):236
30. Wong CJ, Wang L, Holers VM, et al. Elevated plasma complement components in facioscapulohumeral dystrophy. Hum Mol Genet. 2022, Jun, 4;31(11):1821–29
31. Banerji CRS, Greco A, Joosten LAB, van Engelen BGM, Zammit PS. The FSHD muscle-blood biomarker: a circulating transcriptomic biomarker for clinical severity in facioscapulohumeral muscular dystrophy. Brain Commun. 2023, 16;5(5):fcad221
32. Bayazit MB, Henderson D, Nguyen KT, et al. Identification of disease-specific extracellular vesicle-associated plasma protein biomarkers for duchenne muscular dystrophy and facioscapulohumeral muscular dystrophy. medRxiv. [Preprint] 2024. https://doi.org/10.1101/2024.11.29.24317861
33. Qian F, Huang Z, Zhong H, et al. Analysis and biomedical applications of functional cargo in extracellular vesicles. ACS Nano. 2022, 27;16(12):19980–20001
34. Kumar MA, Baba SK, Sadida HQ, et al. Extracellular vesicles as tools and targets in therapy for diseases. Signal Transduct Target Ther. 2024, 5;9(1):27
35. Rome S, Forterre A, Mizgier ML, Bouzakri K. Skeletal muscle-released extracellular vesicles: state of the art. Front Physiol. 2019, Aug, 9;10:929
36. Murphy C, Withrow J, Hunter M, et al. Emerging role of extracellular vesicles in musculoskeletal diseases. Mol Aspects Med. 2018, Apr;60:123–28
37. Catapano F, Scaglioni D, Maresh K, et al. Novel free-circulating and extracellular vesicle-derived miRnas dysregulated in Duchenne muscular dystrophy. Epigenomics. 2020;12(21):1899–915
38. Sandonà M, Consalvi S, Tucciarone L, et al. HDAC inhibitors tune miRnas in extracellular vesicles of dystrophic muscle-resident mesenchymal cells. EMBO Rep. 2020, 3;21(9):e50863
39. Uto K, Ueda K, Okano T, et al. Identification of plexin D1 on circulating extracellular vesicles as a potential biomarker of polymyositis and dermatomyositis. Rheumatol (Oxford). 2022, 11;61(4):1669–79
40. Patel H, Syddall HE, Martin HJ, Cooper C, Stewart C, Sayer AA. The feasibility and acceptability of muscle biopsy in epidemiological studies: findings from the Hertfordshire Sarcopenia study (HSS). J Nutr Health Aging. 2011;15:10–15
41. Fischer D, Kley RA, Strach K, et al. Distinct muscle imaging patterns in myofibrillar myopathies. Neurology. 2008;71(10):758–65
42. Théry C, Witwer KW, Aikawa E, et al. Minimal information for studies of extracellular vesicles 2018 (MISEV2018): a position statement of the International society for extracellular vesicles and update of the MISEV2014 guidelines. J Extracell Vesicles. 2018, Nov, 23;7(1):1535750
43. Aparicio-Puerta E, Gómez-Martín C, Giannoukakos S, et al. sRnabench and sRnatoolbox 2022 update: accurate miRNA and sncRNA profiling for model and non-model organisms. Nucleic Acids Res. 2022, Jul;5(50):(W1): W710–W717
44. Martin M. Cutadapt removes adapter sequences from high-throughput sequencing rreads. EMBnet.journal. 2011, may;17(1):pp. 10–12. ISSN 2226-6089
45. Dobin A, Davis CA, Schlesinger F, et al. STAR: ultrafast universal RNA-seq aligner. Bioinformatics. 2013, Jan, 1;29(1):15–21
46. Dellar ER, Hill C, Melling GE, Carter DRF, Baena-Lopez LA. Unpacking extracellular vesicles: RNA cargo loading and function. J Extracell Biol. 2022, May, 2;1(5):e40
47. Dmitriev P, Stankevicins L, Ansseau E, Petrov A, Barat A, Dessen P, et al. Defective regulation of microRNA target genes inmyoblasts from facioscapulohumeral dystrophy patients. J Biol Chem. 2013;288(49):34989–35002.
48. Chen P, Li Y, Li L, Yu Q, Chao K, Zhou G, Qiu Y, Feng R, Huang S, He Y, Chen B, Chen M, Zeng Z, Zhang S. Circulating microRNA-146b-5p is superior to C-reactive protein as a novel biomarker for monitoring inflammatory bowel disease. Aliment Pharmacol Ther. 2019 Mar;49(6):733–743
49. Kinder TB, Heier CR, Tully CB, et al. Muscle weakness in myositis: MicroRNA-mediated dystrophin reduction in a myositis Mouse model and human muscle biopsies. Arthritis Rheumatol. 2020, Jul;72(7):1170–83
50. Ye L, Zuo Y, Yang H, et al. Specific autoantibodies and clinical phenotypes correlate with the aberrant expression of immune-related MicroRNAs in dermatomyositis. J Immunol Res. 2019; 2019, Feb, 19;2927061
51. Jiang T, Huang Y, Liu H, et al. Reduced miR-146a Promotes REG3A expression and macrophage migration in polymyositis and dermatomyositis. Front Immunol. 2020;11:37
52. Aksu-Menges E, Akkaya-Ulum YZ, Dayangac-Erden D, et al. The common miRNA signatures associated with mitochondrial dysfunction in different muscular dystrophies. Am J Pathol. 2020, Oct;190(10):2136–45
53. Wijnbergen D, Johari M, Ozisik O, et al. Multi-omics analysis in inclusion body myositis identifies mir-16 responsible for HLA overexpression. Orphanet J Rare Dis. 2025, Jan, 15;20(1):27
54. Vonhögen IGC, El Azzouzi H, Olieslagers S, et al. MiR-337-3p Promotes adipocyte browning by inhibiting TWIST1. Cells. 2020, Apr, 23;9(4):1056
55. Yang X, Li Z, Wang Z, Yu J, Ma M, Nie Q. miR-27b-3p attenuates muscle atrophy by targeting Cbl-b in skeletal muscles. Biomolecules. 2022, Jan, 23;12(2):191
56. Yao H, Qian J, Bian XT, Guo L, Tang KL, Tao X. miR-27b-3p reduces muscle fibrosis during chronic skeletal muscle injury by targeting TGF-βR1/Smad pathway. J Orthop Surg Res. 2024, Jun, 2;19(1):329
57. Wagner V, Meese E, Keller A. The intricacies of isomiRs: from classification to clinical relevance. Trends Genet. 2024, Sep;40(9):784–96
58. Sk W, Ec K, Rk P, Br F, Dw L, Lm D, et al. Post-transcriptional generation of miRNA variants by multiple nucleotidyl transferases contributes to miRNA transcriptome complexity. Genome Res. 2011 Sep;21(9):1450–61
59. Guo L, Zhao Y, Yang S, Zhang H, Chen F. A genome-wide screen for non-template nucleotides and isomiR repertoires in miRNAs indicates dynamic and versatile microRnaome. Mol Biol Rep. 2014, Oct;41(10):6649–58
60. Cui L, Ma R, Cai J, et al. RNA modifications: importance in immune cell biology and related diseases. Sig Transduct Target Ther. 2022;7:334
61. Menning M, Kufer TA. A role for the Ankyrin repeat containing protein Ankrd17 in Nod1- and Nod2-mediated inflammatory responses. FEBS Lett. 2013, Jul, 11;587(14):2137–42
62. Lee KG, Hong BK, Lee S, et al. Nuclear receptor coactivator 6 is a critical regulator of NLRP3 inflammasome activation and gouty arthritis. Cell Mol Immunol. 2024;21:227–44
63. Yin M, Wang X, Lu J. Advances in IKBKE as a potential target for cancer therapy. Cancer Med. 2020, Jan;9(1):247–58

64. Harrod TR, Justement LB. Evaluating function of transmembrane protein tyrosine phosphatase CD148 in lymphocyte biology. Immunol Res. 2002;26(1–3):153–66
65. Yadava RS, Frenzel-McCardell CD, Yu Q, et al. RNA toxicity in myotonic muscular dystrophy induces NKX2-5 expression. Nat Genet. 2008, Jan;40(1):61–68
66. Gudde AEEG, van Heeringen SJ, de Oude AI, et al. Antisense transcription of the myotonic dystrophy locus yields low-abundant RNAs with and without (Cag)n repeat. RNA Biol. 2017, Oct, 3;14(10):1374–88
67. Watanabe M, Ochi H, Arahata H, et al. Myopathy in autoimmune polyendocrinopathy-candidiasis-ectodermal dystrophy. Muscle Nerve. 2012, Jun;45(6):904–08
68. Naguibneva I, Ameyar-Zazoua M, Polesskaya A, et al. The microRNA miR-181 targets the homeobox protein hox-A11 during mammalian myoblast differentiation. Nat Cell Biol. 2006, Mar;8(3):278–84
69. Hudson MB, Woodworth-Hobbs ME, Zheng B, et al. miR-23a is decreased during muscle atrophy by a mechanism that includes calcineurin signaling and exosome-mediated export. Am J Physiol Cell Physiol. 2014, Mar, 15;306(6):C551–8
70. Arrighi N, Moratal C, Savary G, et al. The FibromiR miR-214-3p is upregulated in Duchenne muscular dystrophy and Promotes differentiation of human fibro-adipogenic muscle progenitors. Cells. 2021, Jul, 20;10(7):1832
71. Fiorillo AA, Heier CR, Novak JS, et al. TNF-α-induced microRNAs control Dystrophin expression in becker muscular dystrophy. Cell Rep. 2015, Sep, 8;12(10):1678–90
72. Guess MG, Barthel KK, Harrison BC, Leinwand LA. miR-30 family microRNAs regulate myogenic differentiation and provide negative feedback on the microRNA pathway. PLoS One. 2015, Feb, 17;10(2):e0118229
73. Li N, Zhang L, Guo Q, et al. Aerobic exercise improves inflammation and insulin resistance in skeletal muscle by regulating miR-221-3p via JAK/STAT signaling pathway. Front Physiol. 2025, Feb, 25;16:1534911
74. Wang Z, Li Q, Chamba Y, et al. Identification of genes related to growth and lipid deposition from transcriptome profiles of pig muscle tissue. PLoS One. 2015, Oct, 27;10(10):e0141138
75. Hodgkinson CP, Naidoo V, Patti KG, et al. Abi3bp is a multifunctional autocrine/paracrine factor that regulates mesenchymal stem cell biology. STEM Cells. 2013, Aug;31(8):1669–82
76. Jackson RM, Griesel BA, Short KR, Sparling D, Freeman WM, Olson AL. Weight loss results in increased expression of anti-inflammatory protein CRISPLD2 in Mouse adipose tissue. Obes (Silver Spring). 2019, Dec;27(12):2025–36
77. Wang X, Wang HY, Hu GS, et al. DDB1 binds histone reader BRWD3 to activate the transcriptional cascade in adipogenesis and promote onset of obesity. Cell Rep. 2021, Jun, 22;35(12):109281
78. Fathzadeh M, Li J, Rao A, et al. FAM13A affects body fat distribution and adipocyte function. Nat Commun. 2020, Mar, 19;11(1):1465
79. Longo M, Raciti GA, Zatterale F, et al. Epigenetic modifications of the Zfp/ZNF423 gene control murine adipogenic commitment and are dysregulated in human hypertrophic obesity. Diabetologia. 2018, Feb;61(2):369–80
80. Griffin MJ, Zhou Y, Kang S, Zhang X, Mikkelsen TS, Rosen ED. Early B-cell factor-1 (EBF1) is a key regulator of metabolic and inflammatory signaling pathways in mature adipocytes. J Biol Chem. 2013, Dec, 13;288(50):35925–39
81. Guilherme A, Soriano NA, Furcinitti PS, Czech MP. Role of EHD1 and EHBP1 in perinuclear sorting and insulin-regulated GLUT4 recycling in 3T3-L1 adipocytes. J Biol Chem. 2004, Sep, 17;279(38):40062–75
82. Cheedipudi S, Puri D, Saleh A, et al. A fine balance: epigenetic control of cellular quiescence by the tumor suppressor PRDM2/RIZ at a bivalent domain in the cyclin a gene. Nucleic Acids Res. 2015, Jul, 27;43(13):6236–56
83. Elenbaas JS, Jung IH, Coler-Reilly A, Lee PC, Alisio A, Stitziel NO. The emerging Janus face of SVEP1 in development and disease. Trends Mol Med. 2023, Nov;29(11):939–50
84. Mangolini V, Radeghieri A, Piva S, et al. Universal protocol to separate and compare extracellular vesicles from human plasma and skeletal muscle biopsy. bioRxiv [Preprint] 2024. https://doi.org/10.1101/2024.02.19.580950
85. Cui C, Cui Q. The relationship of human tissue microRNAs with those from body fluids. Sci Rep. 2020;10:5644

Publisher's Note